International school on atomic and nuclear heavy ion interactions
Poiana Brasov (Romania) 28 Aug - 8 Sep 1984
CEA-CONF--7403

28 août-8 sept. 1984

FR8500266

Rapport DPh-N Saclay n° 2195 08/1984

FRAGMENTATION PROCESSES IN NUCLEAR REACTIONS

Robert LEGRAIN
Service de Physique Nucléaire - Basse Energie
CEN Saclay
91191 Gif-sur-Yvette Cedex,France

FRAGMENTATION PROCESSES IN NUCLEAR REACTIONS

Robert LEGRAIN
Service de Physique Nucléaire - Basse Energie
CEN Saclay
91191 Gif-sur-Yvette Cedex,France

I. INTRODUCTION

The word fragmentation has been used for, at least, two different processes in nuclear reactions. First in 1956 R. Wolfang et al. [1] have to postulate a new mode of de-excitation, besides spallation and fission, to account for light fragments observed in the interaction of high energy protons (600 MeV to 3 GeV) with lead. This new mode of de-excitation has been termed fragmentation. Then in 1972 H.H. Heckman et al. [2] have observed fragments having the characteristics of projectile fragment in the interaction of 2.1 GeV/u ^{14}N with ^{12}C. Although this process has some similarities with spallation, they called it fragmentation. In the following, I will refer to this process as projectile fragmentation while the former process will be called nuclear fragmentation. In this lecture I will consider these two different aspects of fragmentation but I will also put the emphasis on heavy ion induced reactions.

In section II devoted to projectile fragmentation, are presented the preliminary results of an experiment performed at GANIL (Caen, France) to study peripheral heavy ions induced reactions at intermediate energy namely the reactions : $^{40}Ar + ^{27}Al$ and $^{40}Ar + ^{nat}Ti$ with a 44 MeV/u ^{40}Ar projectile. This experiment is the joint participation of :

J. Barrette, B. Berthier, E. Chavez, D.M. de Castro Rizzo, O. Cisse, R. Dayras, R. Legrain, M.C. Mermaz, A. Pagano, E.C. Pollacco,
from : DPh-N/BE, Saclay

H. Delagrange, W. Mittig,
from : GANIL, Caen

B. Heusch,
from CRN Strasbourg

G. Lanzano, A. Palmeri,
from INFN, Catania, Italy.

The results of this experiment will illustrate the characteristics of projectile fragmentation and this will also give the opportunity to study projectile fragmentation in the transition region.

In Section III I will consider nuclear fragmentation which is associated with more central collisions in the case of heavy ion induced reactions. I will also illustrate this aspect of fragmentation with two heavy ion experiments in which fragments emitted at large angle have been observed :

1) the reaction $^{20}Ne + ^{197}Au$ with a 38 MeV/u ^{20}Ne projectile performed at SARA, Grenoble, France. It has been achieved by the joint participation of :

Y. Cassagnou, M. Conjeaud, S. Harar, R. Legrain, E. Pollacco, C. Volant from DPh.N/BE, Saclay.

J. Menet, J.B. Viano
from I.S.N. Grenoble.

2) the reaction $^{40}Ar + ^{197}Au$ with a 44 MeV/u ^{40}Ar projectile performed at GANIL, Caen, France with the joint participation of :

Y. Cassagnou, D.M. de Castro-Rizzo, R. Dayras, R. Legrain,

L. Rodriguez, N. Saunier
from DPH.N/BE, Saclay.

M.G. Saint-Laurent
from GANIL, Caen.

R. Fonte, J. Imme-Raciti, G. Raciti from Catania, Italy.

II. PROJECTILE FRAGMENTATION

II.1. General characteristics

In the seventies, a series of experiments was made at Berkeley using relativistic ^{12}C, ^{16}O refs.[3,4] and ^{40}Ar refs.[5] projectiles. From this work the general characteristics of projectile fragmentation at high energy have emerged :

1) The momentum distribution of projectile fragments can be parametrized in the projectile rest frame as :

$$\frac{d^3\sigma}{d^3p} = C \exp(-P_\perp/2\sigma_\perp^2) \exp(-(P_\parallel - \langle P_\parallel \rangle)^2/2\sigma_\parallel^2) \qquad (1)$$

where $P_\perp$ and $P_\parallel$ are the tranverse and longitudinal momenta of the fragments, $\langle P_\parallel \rangle$ is the value of the shift from zero momentum, which is small

and $\sigma_\perp$ and $\sigma_\parallel$ are the widths for the transverse and longitudinal momentum distributions $\sigma_\parallel = \sigma_\perp$ within 10% [3].

2) The distribution of $\sigma_\parallel$ as a function of fragment mass number F is in agreement with the parabolic form :

$$\sigma_\parallel^2 = \sigma_0^2 \frac{F(A - F)}{A - 1} \qquad (2)$$

with $\sigma_0 = 80 \div 90$ MeV/c, where A is the projectile mass number. This parabolic dependence on fragment mass arises from a variety of theoretical approaches all dependent on simple postulates including momentum conservation [6-8]. A.S. Goldhaber [8] has shown that the reduced momentum width σ_0 could be related to the Fermi momentum P_F in the case of a fast statistical dissociation of the projectile governed by the distribution of nucleon momenta in the projectile before collision. In this case:

$$\sigma_0 = P_F/\sqrt{5} \qquad (3)$$

But in recent years, the basic assumptions of this statistical fragmentation model [8] have been re-examined by G. Bertsch [9], M.J. Murphy [10], and W.A. Friedman [11].

Remaining in the same framework, G. Bertsch and M.J. Murphy have shown that it was necessary to take into account the Pauli principle on the momenta of the nucleons that make up the fragment [9] and the constraints imposed by the requirement that the fragment must be a Fermi gas [10]. With these corrections included the statistical fragmentation model does not reproduce the data any more [10].

With a different approach which emphasizes the peripheral nature of fragmentation reactions, W.A. Friedman claimed that the separation energy (of the fragment and the removed portion of the projectile) and not the Fermi momentum is determining the parallel momentum widths. The parameter of this peripheral model is contained in a cut-off radius x_0 that ensures the peripherality of the reaction. x_0 is parametrized as:

$$x_0 = r_0 A_F^{1/3} \qquad (4)$$

where A_F is the fragment mass number. With $r_0 = 1.2$ fm the agreement with the data for O^{16} and C^{12} projectiles is improved relative to the parabolic law.

A.S. Goldhaber [8] has also shown that on the other hand, if the nucleus comes to equilibrium at temperature T after excitation and then decays to the observed fragment, we have:

$$\sigma_0 = mkTF(A - F)/A \qquad (5)$$

where m is the nucleon mass and k the Boltzmann constant.

3) The fragmentation cross sections are generally reproduced by an abrasion-ablation model [12-13]. In this model, the fragmentation occurs in two steps.

In the first step, the abrasion stage, the overlapping nuclear matter is sheared away from both the target and the projectile. The remaining prefragment is left in an excited state and subsequently decays, this is the ablation stage. Two different approaches have been used to treat the abrasion : the Glauber model [13] and the fireball geometry [12,14] ; both approaches give similar results.

For 2.1 GeV/u ^{16}O projectiles, the widths [15] and the shifts [16] of the momentum distributions have also been reproduced in the framework of the abrasion-ablation model. It should be mentioned that the possibility of observing isospin ground state correlations directly in mass and charge distributions of projectile fragments has been discussed [17,18], but the comparison [19] of an abrasion-ablation model including correlations and of an uncorrelated intranuclear cascade model with available data gives no definite answer since both models are in agreement with experimental results. It has also to be noted that there is evidence for the validity of the geometrical abrasion model of relativistic heavy ions [20]. This has been obtained by comparing the distributions of summed projectile masses for 2.1 GeV/u ^{20}Ne on ^{12}C and ^{20}Ne on Mo measured with a calorimeter and calculated using the abrasion model.

The interest in the energy dependence of projectile fragmentation increased with the measurement [21] of energy spectra of projectile fragments emitted in the reaction of 20 MeV/u ^{16}O on ^{208}Pb similar to energy spectra observed with 2.1 GeV/u projectiles. Furthermore, the relative fragment yields were found remarkably similar at 20 MeV/u and 2.1 GeV/u [22,23]. Since then other experiments have been performed with different projectiles in the energy range 10 ÷ 100 MeV/u [24-34]. It appears that the reduced momentum width σ_0 exhibits a relatively rapid increase in this energy range from a low value below 10 MeV/A to the asymptotic value (80÷90 MeV/c) at relativistic energy. The reasons for this transition are not known

yet but it seems that the high energy regime of projectile fragmentation begins to set in at 40 ÷ 45 MeV/u.

For incident energies lower than ~ 100 MeV/u, $\sigma_{\parallel}$ and $\sigma_{\perp}$ are not found equal any longer. The larger $\sigma_{\perp}$ observed for ^{16}O induced reactions at 90 and 120 MeV/u [31] have been interpreted as being due to the orbital deflection of the projectile in the nuclear and Coulomb potentials of the target. In this case a momentum is transferred to the projectile and the transverse momentum width is given by:

$$\sigma_{\perp}^2 = \frac{F(A - F)}{A - 1} \sigma_0^2 + \frac{F(F - 1)}{A(A - 1)} \sigma_D^2 \qquad (6)$$

where the first term is identical to relation (2) and $\sigma_D^2 = \frac{1}{2} < P_{A\perp}^2 >$ is the variance of the tranverse momentum of the projectile at the time of fragmentation.

Now we are going to look, in more details, at the results of an experiment performed in the transition region.

II.2. Fragmentation of ^{40}Ar at 44 MeV/u

This experiment was performed at the new heavy ion facility GANIL at Caen (France). A 44 MeV/u beam was used to bombard ~ $1mg/cm^2$ thick self-supporting ^{27}Al and ^{nat}Ti targets. Projectile-like fragments were detected in a multi-silicon-detector telescope at angles ranging from 2.5° to 15° and their 1.80 m time-of-flight path was measured providing mass identification. Light-particle energy spectra were also measured between 5° and 60° with two telescopes consisting of two silicon-detectors and a sodium iodide scintillator.

Some of the features of the projectile-like fragments observed in this experiment may be seen in Figs. 1-4. The distribution of produced fragments is very broad and extends from the projectile down to light particles. At the most forward angles, fragments with Z and A greater than those of the projectile are observed (Figs 1-3). As in high energy fragmentation, the energy spectra (Fig.4) are peaked at an energy slighty lower than the energy corresponding to projectile velocity. However these spectra are asymmetric with a low energy tail which is not observed at higher energy. Typical angular distributions for a few fragments produced in the reaction $^{40}Ar + ^{27}Al$ are shown in Fig. 5. They are strongly forward peaked for nuclei near the projectile and broadened as the mass of the fragment decreases.

After integrating over energy and angles, the mass distribution for the reaction $^{40}Ar + ^{27}Al$ is shown on Fig. 6 while Fig. 7 shows the ratio of the mass yields between the two reactions $^{40}Ar + ^{nat}Ti$ and $^{40}Ar + ^{27}Al$
The primary mass distribution predicted by the clean-cut abrasion-ablation model [12,14] and the calculated ratios of the mass yields between the two reactions are also reported on Figs 6 and 7 ; no normalization coefficient has been applied to the calculation. Considering the simplicity of the model and some of its approximations which should be only valid at relativistic energies, the agreement with the data is surprisingly good in the intermediate mass region (~ 20 to ~ 35). For fragments close to the projectile, the excitation energies calculated with simple minded surface consideration in the framework of the liquid drop model are too small, thus prohibiting those fragments to decay by particle emission. This leads to an excess yield for the heaviest fragments. For light fragments, they may be produced by various mechanisms and the disagreement between the calculation and the data does not imply a defect of the model. Obviously, the model cannot reproduce the cross section for fragments heavier than the projectile which are indicative of transfer processes.

In Fig. 8, we have reported the most probable kinetic energy E_F (in MeV/u) of the fragments as a function of their mass. Two trends can be distinguished in the data : a general linear decrease of the energy E_F with the fragment mass and, for fragments with a given Z a much sharper decrease of the energy E_F with the mass of the isotope. In relativistic heavy ion collisions, this velocity shift has been imputed by A. Abul-Magd et al. [16] to a frictional force resulting from the binding energy of the nucleon abraded from the projectile. The application of this model at such a low incident energy as 44 MeV/u is questionable and not straightforward.

Relation (1) can be transformed in the laboratory reference frame to get the double differential cross section :

$$\frac{d^2\sigma}{dE\ d\Omega} = N_0(2E_F F)^{1/2}\exp\left[-F\left(\frac{E_F\sin^2\theta}{\sigma_\perp^2} + \frac{E_F\cos^2\theta - (E_F\bar{E})\cos\theta + \bar{E}}{\sigma_\parallel^2}\right)\right] \qquad (7)$$

which can be directly compared to the laboratory energy spectra. In this expression, F and E_F are the mass and the kinetic energy spectra of the fragment respectively, $\bar{E}$ is the most probable kinetic energy, N_0 is a normalization factor and θ is the laboratory detection angle.

As it has been mentioned earlier in both the $^{40}Ar + ^{27}Al$ and $^{40}Ar + ^{nat}Ti$ reactions, the energy spectra (Fig. 4) display a low energy tail which cannot be explained in the framework of the pure fragmentation model. In the following analysis, it has been assumed that only the high energy component of the spectra may have its origin in fragmentation. In order to extract values of $\sigma_{\parallel}$, the energy spectra were fitted using relation (7) in which $\sigma_{\parallel}$ and $\bar{E}$ were considered as free parameters. To minimize the effect of the transverse momentum $P_{\perp}$ only, the most forward angle (2.5°) was considered. The fits were started on the left of the spectra at an energy corresponding to 80% of the maximum value. The results of these fits are shown for few fragments from the $^{40}Ar + ^{27}Al$ reaction by the light drawn curves of Fig.14

The extracted variances $\sigma_{\parallel}$ are shown in Fig. 9 as a function of the fragment mass. Taking σ_0 = 87 MeV/c, the variances $\sigma_{\parallel}$ are in average well described by the parabolic law given by relation (2) and represented by the full drawn curve of Fig.9. A similar agreement is obtained for the reaction $^{40}Ar + ^{nat}Ti$. Comparing this value of σ_0 = 87 MeV to the evolution of σ_0 with the projectile energy on Fig. 10, it seems that at ~40 MeV/u σ_0 is just reaching its saturating value.
But this value (σ_0 = 87 MeV/c) is of course too high to be compatible with the statistical model of fragmentation [8] including the corrections of G. Bertsch [9] and M.J. Murphy [10]. However it has to be pointed out that the peripheral model of W.A. Friedman [11] yields too high σ_0 values with the usual value of the parameter r_0 (r_0 = 1.2 fm). It is necessary to use much lower values of r_0 (r_0 = 0.5 ÷ 0.6 fm) in order to get reasonable agreement with the ^{40}Ar data. But these quite small values of r_0 are not really in agreement with the peripherical characteristic of the model.

After integration over energy relation (7) can be used to fit the angular distributions of the fragments. To do so it has been assumed that $\sigma_{\parallel}$ was given by relation (2) with σ_o = 87 MeV/c whereas $\sigma_{\perp}$ was considered as a parameter to be adjusted to fit the data. When considering the whole measured angular range, it was not possible, by using relation (7), to get a good fit to the angular distributions. This suggests again that other mechanisms than fragmentation may contribute to the production of projectile-like fragments. Thus we have limited the fits to the most forward angles ($\theta < 6°$) where fragmentation should dominate. Few examples of those fits are shown in Fig. 5. On Fig. 11, the extracted values of $\sigma_{\perp}$ as a function of the fragment mass are presented. In sharp contrast with

relativistic energy data, for a given fragment, $\sigma_\perp$ is much larger than $\sigma_\parallel$ as already observed in the fragmentation of ^{16}O at 90 and 120 MeV/u [31].

Thus taking into account the orbital dispersion of the projectile in the combined Coulomb and nuclear target fields, we tried to reproduce the data using relation (6) . However as illustrated by Fig. 11, it not possible to find a value of the variance σ_D (due to orbital dispersion) reproducing the data.

Another difference with higher energy data has to be noted. It has been observed [35] for different projectiles at E/A ≈ 100 MeV/u that, for fragments with the same mass A but different atomic number Z, the variance $\sigma_\perp$ decreases slightly but systematically as Z increases. This effect was imputed to a Coulomb final state interaction between the fragments and the protons dissociated from the projectile. In the present case for fragment with mass greater than 20, exactly the opposite effect is observed and it seemed difficult to be explained with a Coulomb final state interaction.

Finally it is also possible to get some information on projectile fragmentation from the light particle measurement. For example alpha particle spectra obtained at angles from 5° to 60° are presented on Fig. 12. These spectra have been analysed in terms of moving thermal sources, actually two sources have been necessary to fit the data as shown by the full drawn curve on Fig. 12. Each source was parametrized as follows [36]:

$$\frac{d^2\sigma}{d\Omega\, dE} = N_0(E - ZE_C)^{1/2} \exp[-(E - ZE_C + E_1 - 2E_1^{1/2}(E - ZE_C)^{1/2}\cos\theta)/T] \quad (8)$$

Here E_C is the kinetic energy gained by the light particle due to the Coulomb repulsion from the remnant of the target, $E_1 = mv^2/2$ is the kinetic energy of a particle at rest in the moving frame, T is the source temperature, θ is the detection angle and N_0 is an overall normalization constant.

In this case we took $E_C = 0$ and we obtained a high velocity source (v/c = 0.238, T = 8.75 MeV) and a low velocity source (v/c = 0.111, T = 11.3 MeV). The low velocity source is the usual source observed in light particle emission at large angles [36] and its characteristics fit quite well the existing systematics. The velocity of the high velocity source is close to the projectile velocity and according to relation (5) T = 8.75 Mev yields σ_0 = 89 MeV/c. This is obviously a fragmentation source. Furthermore, the discrepancy between the fit and the data at 5°, 10° and 15° can be reproduc-

ed by an additional source simulating the decay of projectile pre-fragments. The parameters of this source are : v/c = 0.294 and T = 4.09 MeV. This temperature would correspond to an excitation energy of ~ 60 MeV for pre-fragment of mass 30. This is a further confirmation of the existence of a two-step mechanism in projectile fragmentation.

II.3. Summary

Many features of the high energy fragmentation-like fragments having velocities close to the projectile velocity and momentum width close to the saturation value are present at 44 MeV/U, however several aspects such as energy dissipation and transfer processes are reminiscent of a low energy behaviour.

The abrasion-ablation model which is in agreement with data at high energy gives surprisingly good results when compared to 44 MeV/u data.

A satisfactory unified description of the momentum distribution of projectile fragments that includes the transition region remains to be developed.

III. NUCLEAR FRAGMENTATION

III.1 Introduction

The interest in nuclear fragmentation has been recently renewed by the interpretation of the fragment emission in high energy protons (80 to 350 GeV) induced reactions as a critical phenomenon [37-39]. At the same time, the possibility of existence of a liquid-gas phase transition [40-45] and more generally the evolution of the initially heated zone (fireball) [46,47] in fragmentation reactions was considered theoretically. In analogy with the condensation theory of Fisher [48] which predicts the distribution of droplets of size A from a condensed vapour at the critical point to be:

$$P(A) \sim A^{-\tau} \qquad (9)$$

It has been suggested [37,49] that this power law dependence with $\tau = 2 \div 3$ may constitute a signature for the occurence of phase transition phenomena near the critical point. But A.D. Panagiotou et al. [50] have fitted the fragment distributions from various reactions [31,51-54] with a power law dependence and plotted the apparent exponent obtained from this analysis as

a function of the temperature of the system (Fig. 13). They have associated the minimum value of the apparent exponent with the critical temperature T_c yielding $T_c = 11 \div 12$ MeV. Although D.H. Boal [55] found some ambiguities in this analysis, it is interesting to note that the critical temperature would be in a range easily obtained with intermediate energy heavy ions.

Alternative models for the fragment emission in heavy ions induced reactions also exist. They are based either on a statistical and chemical equilibrium picture [56,57] or they assume that the fragments come from the remnant of the target which breaks into many pieces in the more central collisions while only minimal statistical assumptions are made [58-61]. Let us now look at the results of two experiments for which any of these models could be valid

III.2. Fragmentation emission in $^{20}Ne + ^{197}Au$ and $^{40}Ar + ^{197}Au$ reactions

Fragments emitted at large angles have been detected in a silicon detector telescope in two different experiments. In the experiment performed at GANIL using a 44 MeV/n ^{40}Ar beam, the fragments ($5 \leq A \leq 18$) have been isotopically identified but in the experiment performed at SARA with a 38 MeV/n ^{20}Ne beam, only a charge separation has been achieved up to now.

Figs. 14 and 15 show some examples of fragment energy spectra for the two reactions. Two features are prominent on these spectra.

1) The high energy part of the spectra shows a slope which becomes steeper with increasing angle.

2) The maximum observed at low energy is moving to lower energies with increasing angle.

These spectra look similar to the light particle energy spectra which have been successfully fitted with a moving source model [36].

On Figs 16 and 17, contour lines of invariant cross sections are drawn in the velocity plane ($\beta_{\parallel}, \beta_T$). On all these velocity plots a crescent-shaped ridge is prominent at intermediate longitudinal velocity. It is particularly clear in the case of the Ne + Au reaction that a projectile velocity component is deforming the spectra at the most forward angles for fragments such as O and B lighter than the projectile.

An attempt to parametrize the data using the moving thermal source model and relation (8) has been made. The solid lines on Figs. 14 and 15 correspond to the results of such a fit for the Ne + Au reaction ; in order

to avoid a projectile fragmentation contribution only the most backward angles have been included in the fit of the energy spectra for fragments with $Z < 10$, while all the measured angles have been used to fit the spectra of the fragments heavier than the projectile. The fit is only fair ; however the general trend of the data seems to be reproduced. This can also be seen of Fig. 18 which shows the velocity plot resulting from the fitting procedure for the ^{6}Li fragments from the $^{40}Ar + ^{197}Au$ reaction. The shape in the velocity plane is approximately reproduced.

For the $^{40}Ar + ^{197}Au$ reaction, all fragments between mass 6 and 15 were fitted with rather similar values of the two parameters T and v/c as shown on Fig. 19. The Coulomb repulsion from the remnant of the target E_c has been set at 6 MeV per charge since this value gave the best results.

In the case of the $^{20}Ne + ^{197}Au$ reaction (Fig. 20) the value of the temperatures derived from the fit are comparable to those for $^{40}Ar + ^{197}Au$ in the same fragment mass range, but for the heavier fragment there is a significant decrease of the temperature while the source velocity is smoothly decreasing from $Z = 5$ to $Z = 16$.

The similarity of the temperatures over the measured range of fragment masses in the case of the Ar + Au reaction would suggest that the fragments originate from a common thermal source but on the other hand the decrease of the source velocity for the $^{20}Ne + ^{197}Au$ reaction is not consistent with this hypothesis. However the moving source parametrization allows the comparison of different data sets and suggests the Coulomb origin of the particular shape of the velocity plots.

Integrating over angle and energy, the fragment production cross sections are obtained. They are plotted on Figs 21 and 22 as a function of fragment mass for the $^{40}Ar + ^{197}Au$ reaction and as a function of fragment charge for the $^{20}Ne + ^{197}Au$ reaction. Also shown on these figures are fits to the production cross section with relation (9) giving values of τ of 2.30 and 2.31 for the $^{40}Ar + 197Au$ and $^{20}Ne + ^{197}Au$ reactions respectively. But in the condensation theory of Fischer [48] relation (9) is only valid at the critical point. More generally the production of droplets of size A is given by :

$$P(A) = A^{-\tau} \exp[(aA^{2/3} + bA - \mu A)/T] \qquad (10)$$

where $a = a(T)$ is the surface free energy per particle, $b = b(T)$ is the volume free energy per particle and μ is the chemical potential per particle.

If x and y are two quantities defined as follows :

$$x = \exp(-a/T) \tag{11}$$

$$y = \exp(-(b-\mu)/T) \tag{12}$$

then the Fisher law can be rewritten as :

$$P(A) = A^{-\tau} x^{A^{2/3}} y^{A} \tag{13}$$

In the vicinity of the critical point, it can be shown that if $T > T_c$ the surface energy is zero since the droplets disappear into vapour and if $T < T_c$ the volume energy is equal to the chemical potential because the Gibbs free energy is zero.

Then for $T \simeq T_c$ the quantities $x \simeq y \simeq 1$ and the distribution (10) has the simple form of relation (9) ($P(A) = A^{-\tau}$).

In analogy with real gas theory, the nuclear condensation picture predicts a maximum in fragment production and thus a minimum value of τ at the critical point. Fitting the data with relation (9) gives an apparent exponent in which the temperature factors are absorbed. Therefore this apparent exponent varies with temperature as shown on Fig. 13. It can also be seen on Fig. 13 that our data points at mean temperatures 14.4 and 16 MeV for the $^{20}Ne + ^{197}Au$ and $^{40}Ar + ^{197}Au$ reactions respectively, fit quite well the systematic. But it has also to be noted that in heavy ion reactions the critical temperature would be attained below 40 MeV/n incident energy . Nevertheless an excitation function of the fragment distribution spanning the region of the critical temperature with an unique system is really needed.

An alternative model which makes only minimal assumptions [59] can be easily compared to the data. In this model the fragments originate from the target spectator which breaks into pieces and the charge yield curve is given by :

$$\frac{d\sigma}{dZ} = \sigma_F \frac{1}{\exp(1.28\, Z/\sqrt{Z_o}) - 1} \tag{14}$$

In this relation σ is the total fragmentation cross section and Z_o is the charge of the nuclear system the fragments of which are detected.

If Z_P and Z_T are the projectile and target charges respectively, Z_o should be :

$$Z_o = Z_P + Z_T - Z_{fast} \tag{15}$$

Here Z_{fast} are the fast charged particles which are knocked out directly by the high energy projectile :

Only two assumptions have been made to derive formula (14) :

1) Maximal entropy : any possible fragmentation is equally probable.

2) Charge conservation.

It has also to be pointed out that the same formula is valid for the partition of A_o nucleons. The predictions of formula (14) for the fragmentation of a target-size object are compared to our data on Figs. 23 and 24. The calculated distribution is not very sensitive to sensible changes in Z_o and at these low incident energies, Z_o is believed to be large since the projectile may be stopped in the target for small impact parameters and only a part of the geometrically overlapping volume form a fireball or a hot spot.

The contribution of the evaporation coming from peripheral target fragmentation has been approximated following X. Campi et al. [61] by :

$$\sigma_{ev} = \sigma_o \exp(- 0.5\ A_F) \qquad (16)$$

and is also reported on Figs 23 and 24 where the sum of these two components (fragmentation and evaporation) with arbitrary normalization factors is represented by a solid line. The agreement with the data is surprizingly good. But it is only for fragments with $Z \leq 10$ in the case of the Ne + Au reaction that the fragmentation would account for the totality of the fragment cross section.

This makes it difficult to test the predictions of the fragmentation models that are explicitely treating the dynamics of the reactions [60], because only poor statistics are available for the heavier fragments. Better measurements of fragments in the range of masses from 12 to 40 are necessary to be more conclusive on the reaction mechanism.

III.3. Summary.

The general features of the fragments energy spectra can be reproduced by a moving thermal source model.

The fragment production cross sections can be fitted by a power law distribution and the apparent exponent obtained together with the temperature derived from the moving source analysis fits quite well with the systematics of fragment emission in proton or heavy ions induced reactions. This would show that the critical temperature if there is liquid gas phase

instabilities would be attained below 40 MeV/n incident energy in ^{20}Ne or ^{40}Ar induced reactions.

A model of fragmentation of the remnant of the target with minimal assumptions is equally good in reproducing the fragments distribution if one takes into account the evaporation from more peripheral collisions.

Better measurements of fragment production as well as an excitation function spanning the critical region and coincidence experimpents are necessary to elucidate the origin of intermediate mass fragments and to be more conclusive about the existence of liquid gas instabilities.

IV. CONCLUSION

Intermediate energy heavy ion reactions offer at least two interesting problems : the onset of the high energy projectile fragmentation regime and the possible existence of liquid-gas phase instabilities. Many more experiments and calculations will be necessary. But we may learn how much energy a nucleus can absorb before breaking and it may give us a better knowledge of the nuclear equation of state.

Références

[1] R. Wolfgang, E.W. Baker, A.A. Caretto, J.B. Cumming, G. Friedlander, and J.D. Hudis, Phys. Rev 103 (1956) 394

[2] H.H. Heckman, D.E. Greiner, P.J. Lindstrom, and F.S. Bieser, Phys. Rev. Lett. 28 (1972) 926

[3] D.E. Greiner, P.J. Lindstrom, H.H. Heckman, B. Cook, and F.S. Bieser, Phys. Rev. Lett. 35 (1975) 152

[4] D.L. Olson, B.L. Berman, D.E. Greiner, H.H. Heckman, P.J. Lindstrom, and H.J. Crawford, Phys. Rev. C28 (1983) 1602

[5] Y.P. Viyogi, T.J.M. Symons, P. Doll, D.E. Greiner, H.H. Heckman, D.L. Hendrie, P.J. Lindstrom, J. Mahoney, D.K. Scott, K. Van Bibber, H. Wieman, H.J. Crawford, C. McParland, and C.K. Gelbke, Phys. Rev. Lett. 42 (1979) 33

[6] H. Feschbach and K. Huang, Phys. Lett. 47B (1973) 300

[7] J.V. Lepore and R.J. Ridell, Rep. LBL 3086 (1974)

[8] A.S. Goldhaber, Phys. Lett. 53B (1974) 306

[9] G. Bertsch, Phys. Rev. Lett. 46 (1981) 47

[10] M.J. Murphy, Phys. Lett. 135B (1984) 25

[11] W.A. Friedman, Phys. Rev. C27 (1983) 569

[12] J.D. Bowman, W.J. Swiatecki, and C.F. Tsang, Rep. LBL 2908 (1973)

[13] J. Hüfner, K. Schäfer, and B. Schürmann, Phys. Rev. C12 (1975) 1888

[14] L.F. Oliveira, R. Donagelo, and J.O. Rasmussen, Phys. Rev. C19 (1979) 826

[15] A. Abul Magd, and J. Hufner, Z. Phys. A277 (1976) 379

[16] A. Abul Magd, J. Hüfner, and B. Schürmann, Phys. Lett. 60B (1976) 327

[17] J. Bondorf, G. Fai, and O.B. Nielsen, Phys. Rev. Lett. 41 (1978) 391

[18] J. Bondorf, G. Fai, and O.B. Nielsen, Nucl. Phys. A312 (1978) 149

[19] D.J. Morissey, L.F. Oliveira, J.O. Rasmussen, G.T. Seaborg, Y. Yariv, and Z. Fraenkel, Phys. Rev. Lett. 43 (1979) 1139

[20] J.D.Stevenson, J. Martinis, and P.B. Price, Phys. Rev. Lett. 47 (1981) 990

[21] C.K. Gelbke, D.K. Scott, M. Bini, D.L. Hendrie, J.L. Laville, J.Mahoney, M.C. Mermaz, and C. Olmer, Phys. Lett. 70B (1977) 415

[22] M. Buenerd, C.K. Gelbke, B.G. Harvey, D.L. Hendrie, J. Mahoney, A. Menchaca-Rocha, C. Olmer, and D.K. Scott, Phys. Rev. Lett. 37 (1976) 1191

[23] C.K. Gelbke. M. Buenerd, D.L. Hendrie, J. Mahoney, M.C. Mermaz, C. Olmer,and D.K. Scott, Phys. Lett. 65B (1976) 227

[24] Ch. Egelhaaf, G. Bohlen, H. Fuchs, A. Gamp, H. Homeyer, and H. Kluge, Phys. Rev. Lett. 46 (1981) 83

[25] B.G. Harvey, Phys. Rev. Lett. (comments) 47 (1981) 454

[26] J.B. Natowitz, M.N. Namboodiri, L. Adler, R.P. Schmitt, S. Simon, M.Berlanger, and R. Choudhury, Phys. Rev. Lett. 47 (1981) 1114

[27] M. Murphy, and R.G. Stokstad, Phys. Rev. C28 (1983) 428

[28] M.N. Namboodiri, R.K. Choudhury, J.B. Natowitz, K. Hagel, L. Adler, P.L. Gonthier, H. Simon, S. Kniffen, R. Patton, E. Tomasi, C. Ngô, C. Mazur, and M. Ribrag, Phys. Rev. C28 (1983) 460

[29] J. Mougey, R. Ost, M. Buenerd, A.J. Cole, C. Guet, D. Lebrun, J.M. Loiseaux, P. Martin, M. Maurel, E. Monnand, H. Nifenecker, P. Perrin, J. Pinston, C. Ristori, P. de Saintignon, F. Schussler, L. Carlen, B. Jakobsson, A. Oskarsson, I.Otterlund, B. Schroder, H.A. Gustafsson, T. Johansson, H. Ryde, J.P. Bondorf, O.B. Nielsen, G. Tibell, Phys. Lett. 105B (1981) 25

[30] J. Barrette, B. Berthier, E. Chavez, O. Cisse, R. Dayras, R. Legrain, M.C. Mermaz, A. Pagano, E. Pollacco, M. Delagrange, W. Mittig, B. Heusch, G. Lanzano, and A. Palmeri, Rapporb DPh-N Saclay n° 21351 and Proc. XXIInd Int. Winter Meeting on nuclear physics, Bormio (1984)

[31] K. Van Bibber, D.L. Hendrie, D.K. Scott, H.H. Wieman, L.S. Shroeder, J.V. Geaga, S.A. Chessin, R.T. Treuhaft, Y.J. Grossiord, J.O. Rasmussen, and C.Y. Wong, Phys. Rev. Lett. 43 (1979) 840

[32] A. Menchaca-Rocha, M.E. Brandan, M. Buenerd, J. Chauvin, D. Lebrun, P. Martin, P. de Saintignon, J.C. Gondrand, I. Dorion, and A.Lounis, Phys. Lett. 131B (1983) 31

[33] D. Guerreau, V. Borrel, D. Jacquet, J. Galin, B. Gatty, and X. Tarrago, Phys. Lett. 131B (1983) 293

[34] V. Borrel, D. Guerreau, J. Galin, B. Gatty, D. Jacquet, and X. Tarrago, Z. Phys. A314 (1983) 191

[35] C.Y. Wong and K. Van Bibber, Phys. Rev. C25 (1982) 2990

[36] T.C. Awes, S.Saini, G. Poggi, C.K. Gelbke, D. Cha, R. Legrain, and G.P. Westfall, Phys. Rev. C25 (1982) 2361

[37] J.E. Finn, S. Agarwal, A. Bujak, J. Chuang, L.J. Gutay, A.S. Hirsch, R.W. Minich, N.T. Porile, R.P. Scharenberg, B.C. Stringfellow, and F. Turkot, Phys. Rev. Lett. 49 (1982) 1321

[38] R.W. Minich, S. Agarwal, A. Bujak, J. Chuang, J.E. Finn, L.J. Gutay, A.S. Hirsch, N.T. Porile, R.P. Scharenberg, B.C. Stringfellow, and F. Turkot, Phys. Lett. 118B (1982) 458

[39] A.S. Hirsch, A. Bujak, J.E. Finn, L.J. Gutay, R.W. Minich, N.T. Porile, R.P. Scharenberg, B.C. Stringfellow, and F. Turkot, Phys. Rev. C29 (1984) 508

[40] H. Schulz, L. Munchow, G. Röpke,and H. Schmidt, Phys. Lett. 119B (1982) 12

[41] P.J. Siemens, Nature 305 (1983) 410

[42] M.W. Curtin, H. Toki, and D.K. Scott, Phys. Lett. 123B (1983) 289

[43] H. Jaqaman, A.Z. Mekjian, and L. Zamick, Phys. Rev. C27 (1983) 2782

[44] H. Schulz, D.N. Voskresensky, and J. Bondorf, Phys. Lett. 133B (1983) 141

[45] H. Jaqaman, A.Z. Mekjian, and L. Zamick, Phys. Rev. C29 (1983) 2067

[46] G. Bertsch, and P.J. Siemens, Phys. Lett. 126B (1983) 9

[47] J. Cugnon, Phys. Lett. 135B (1984) 374

[48] M. Fisher, Physics 3 (1967) 255

[49] C.B. Chitwood, D.J. Fields, C.K. Gelbke, W.G. Lynch, A.D. Panagiotou, M.B. Tsang, H. Utsunomiya, and W.A. Friedman, Phys. Lett. 131B (1983) 289

[50] A.D. Panagiotou, M.W. Curtin, H. Toki, D.K. Scott, and P.J. Siemens, Phys. Rev. Lett. 52 (1984) 496

[51] R.E.L Green, and R.R. Korteling, Phys. Rev. C22 (1980) 1594

[52] R.E.L Green, R.R. Korteling, and K.P. Jackson, Report TRI-PP-83-118

[53] G.D. Westfall, R.G. Sextro, A.M. Poskanzer, A.M. Zebelman, G.W. Butler, and E.K. Hyde, Phys. Rev. C17 (1978) 1368

[54] A.M. Poskander, G.W. Butler, and E.K. Hyde, Phys. Rev. C3 (1971) 882

[55] D.H. Boal, Phys. Rev. C30 (1984) 119

[56] G. Fai, and J. Randrup, Nucl. Phys. A381 (1982) 557

[57] D.H.E. Gross, L. Satpathy, Meng Ta-Chung, M. Satpathy, Z. Phys. A309 (1982) 41

[58] J.P. Bondorf, Nucl. Phys. A387 (1982) 25c

[59] J. Aichelin, and J. Hüfner, Phys. Lett. 136B (1984) 15

[60] J. Aichelin, J. Hüfner, and R. Ibarra, Phys. Rev. C30 (1984) 107

[61] X. Campi, J. Desbois, and E. Lipparini, Phys. Lett. 142B (1984) 8

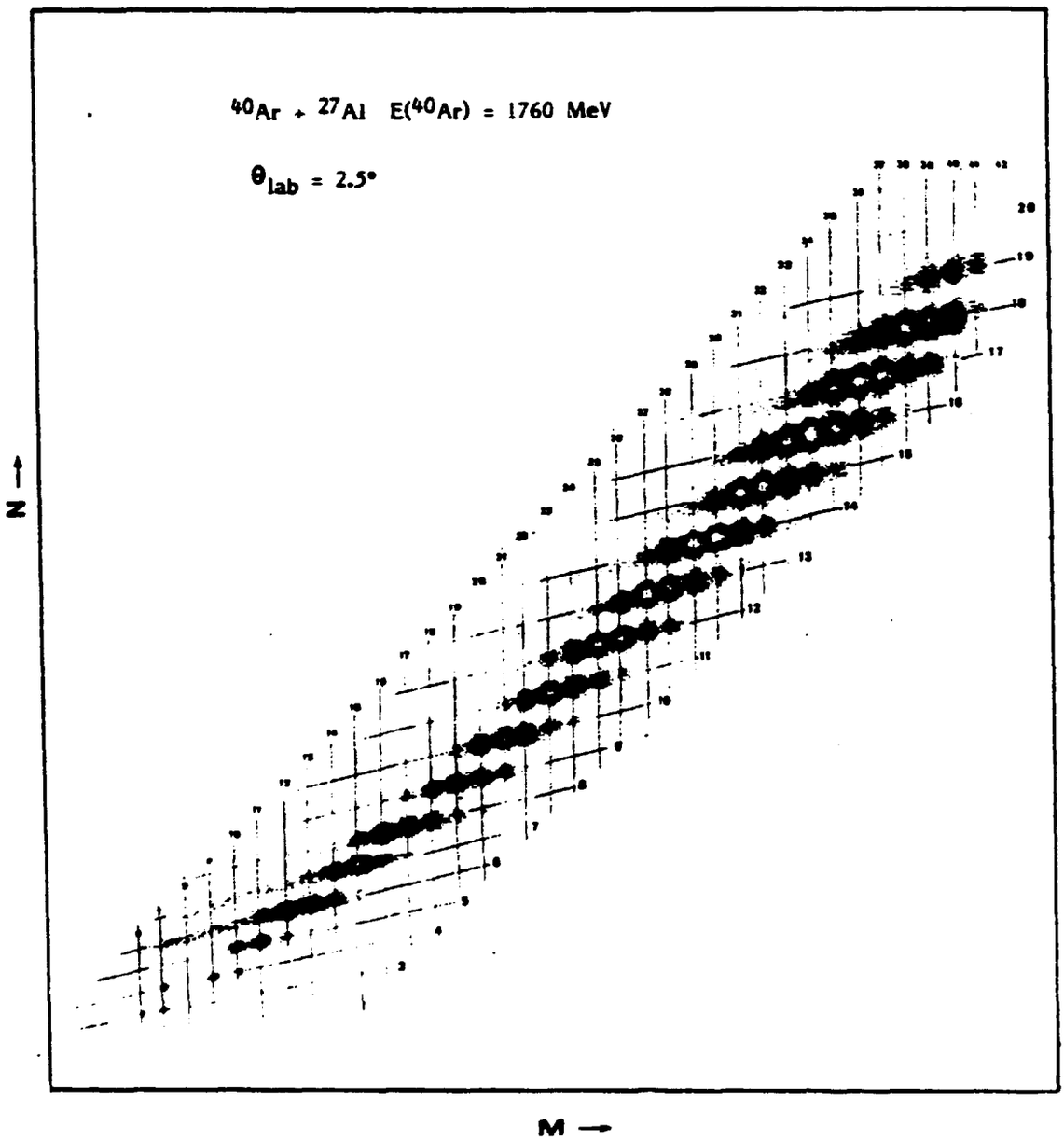

Fig. 1 : Distribution of the projectile-like fragments in the Z vs M plane at 2.5° in the reaction $^{40}Ar + ^{27}Al$.

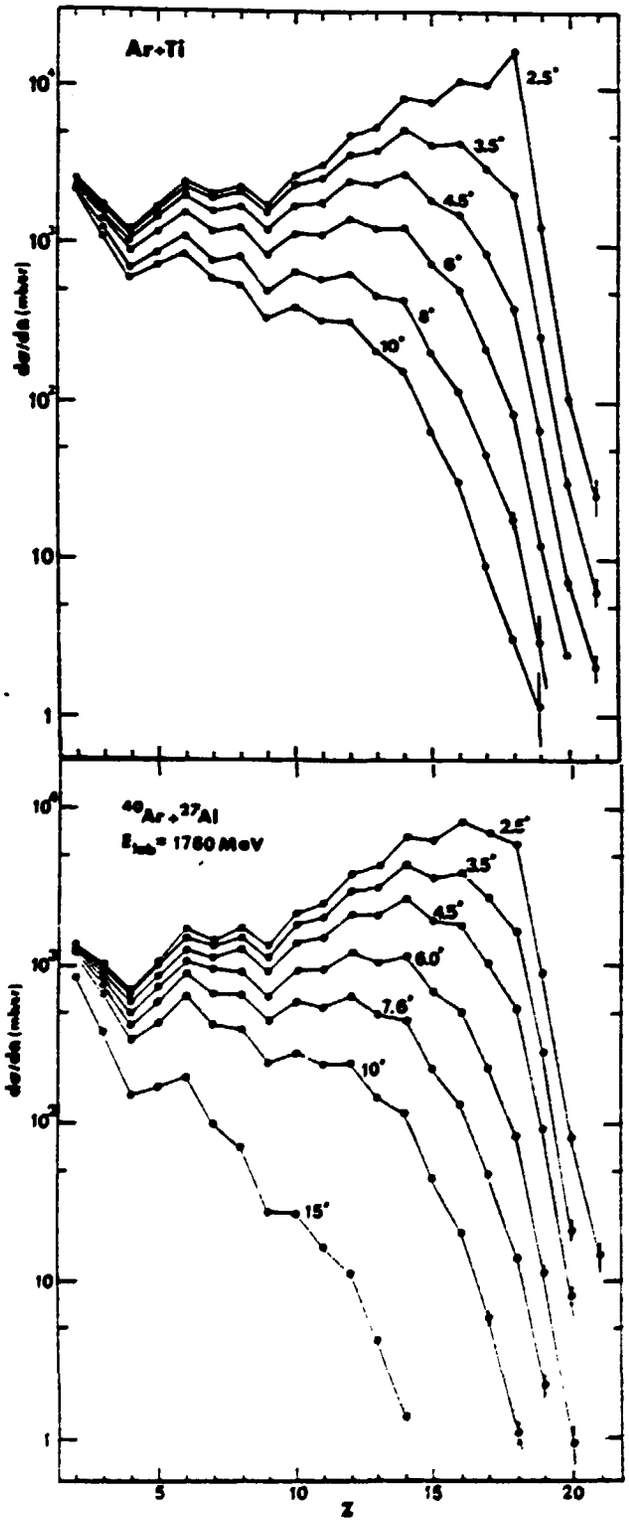

Fig. 2 : Z-distributions of the fragments as a function of detection angle for the reaction $^{40}Ar + ^{nat}Ti$ (a) and the reaction $^{40}Ar + ^{27}Al$ (b).

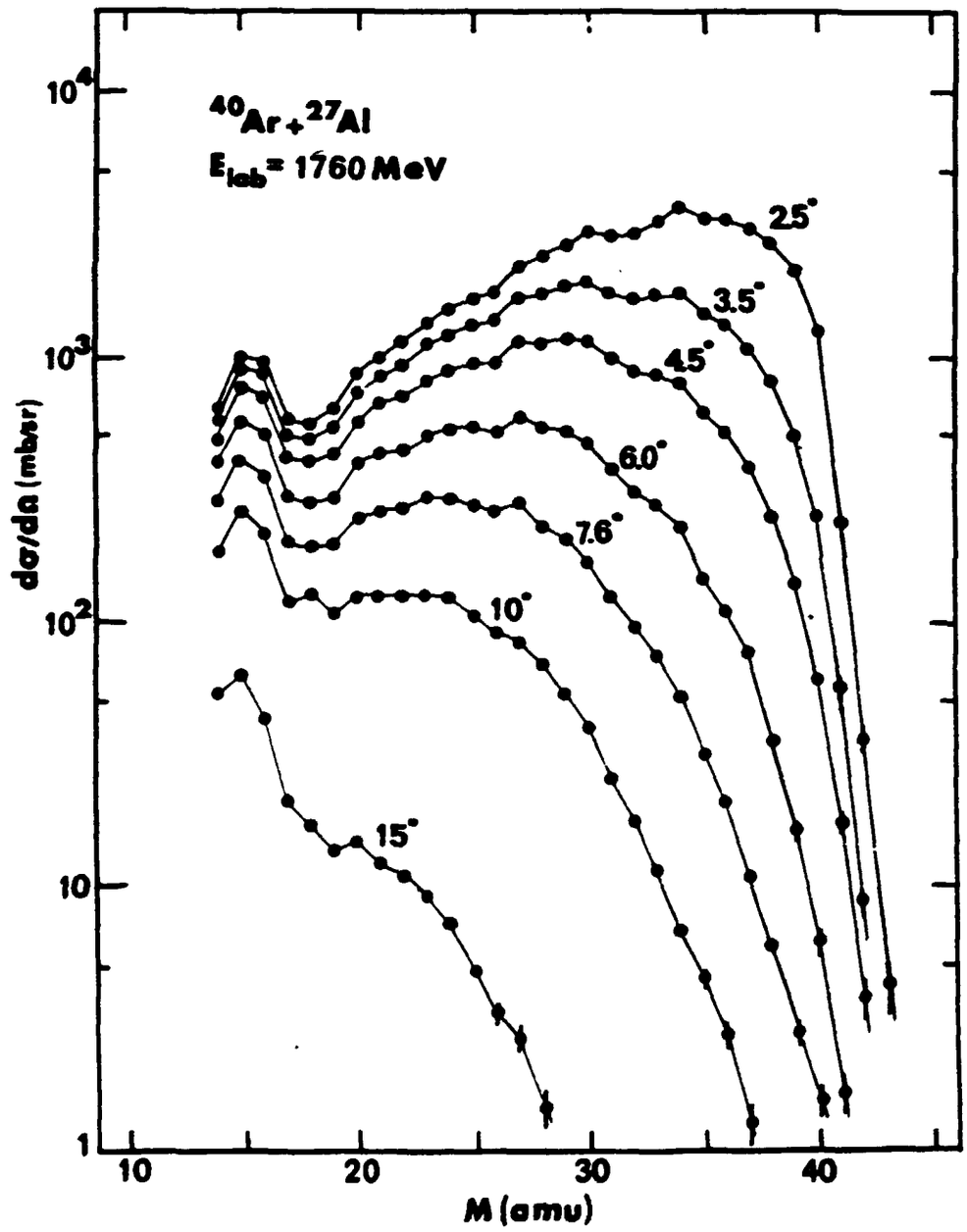

Fig. 3 : M-distributions of the fragments as a function of detection angle for the reaction $^{40}Ar + ^{27}Al$.

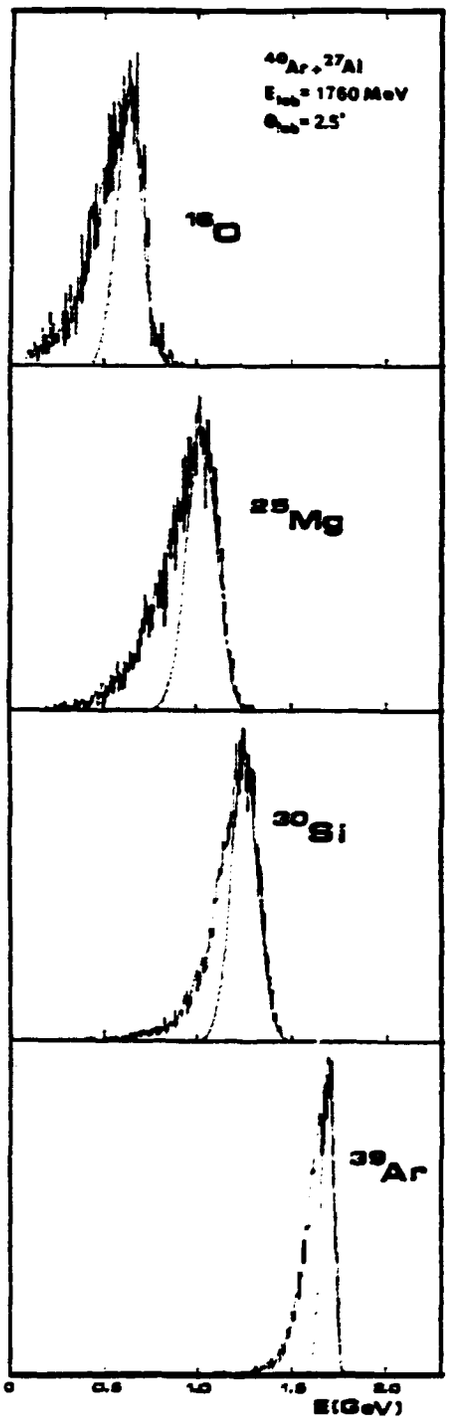

Fig. 4 : Sample of energy spectra in the laboratory for few isotopes produced in the reaction $^{40}Ar + ^{27}Al$. The solid lines are fits to the data using relation (7).

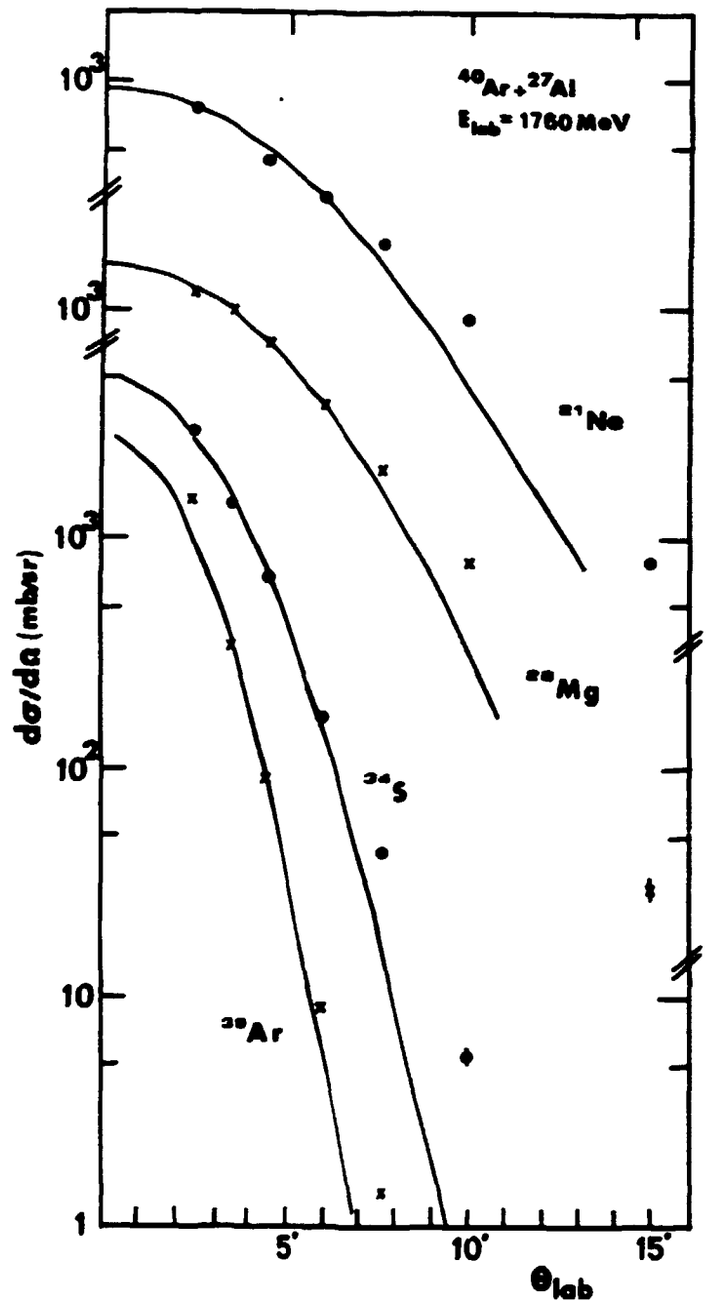

Fig. 5 : Angular distributions of projectile-like fragments after integration over all energies. The curves are fits to the data using relation (7).

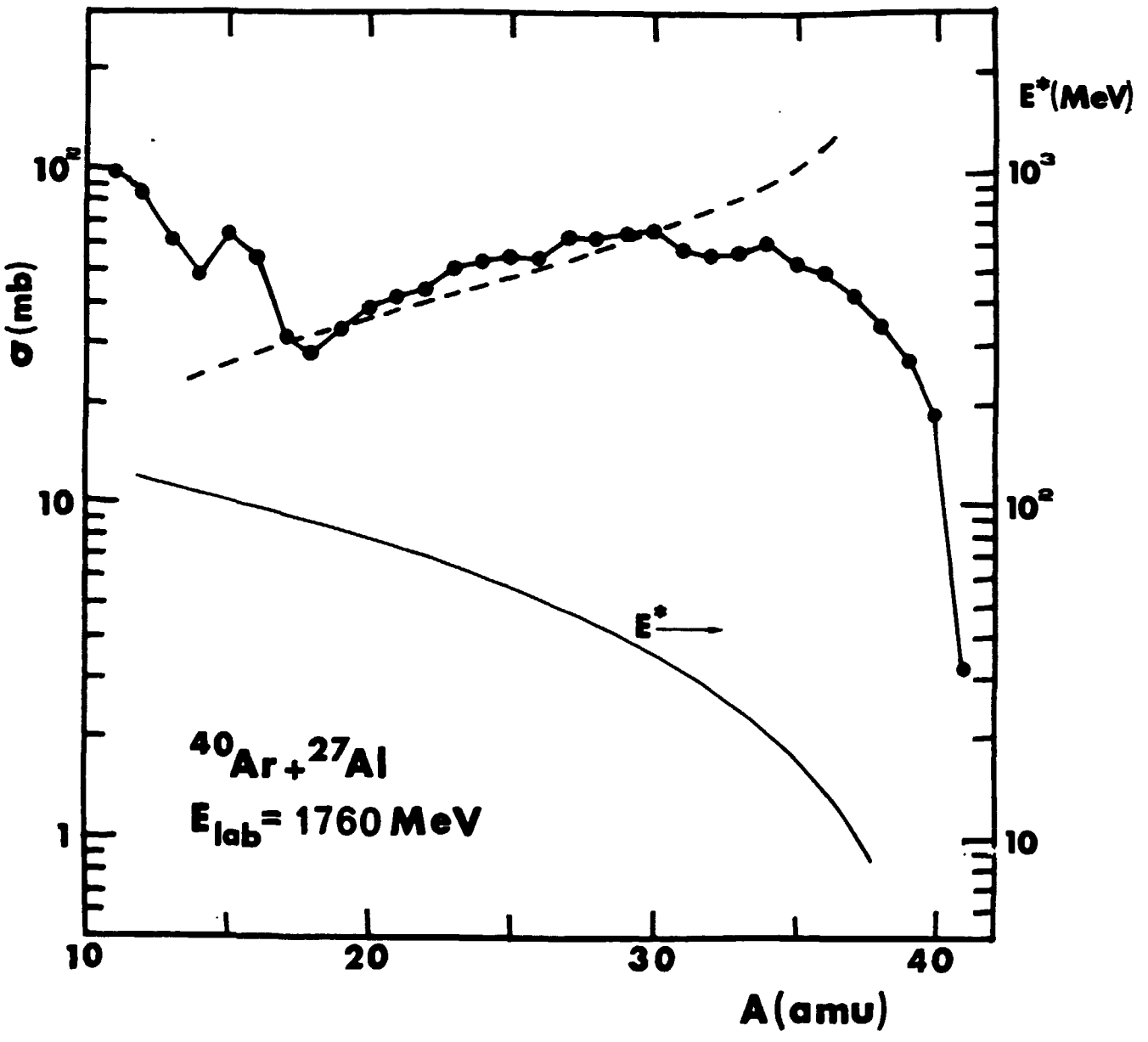

Fig. 6 : M-distributions of the fragments integrated over energies and angles for the reaction $^{40}Ar + ^{27}Al$. The dashed line is the M-distribution predicted by a clean cut abrasion calculation. The solid line is the excitation energy (right scale) of the fragments predicted by the calculation.

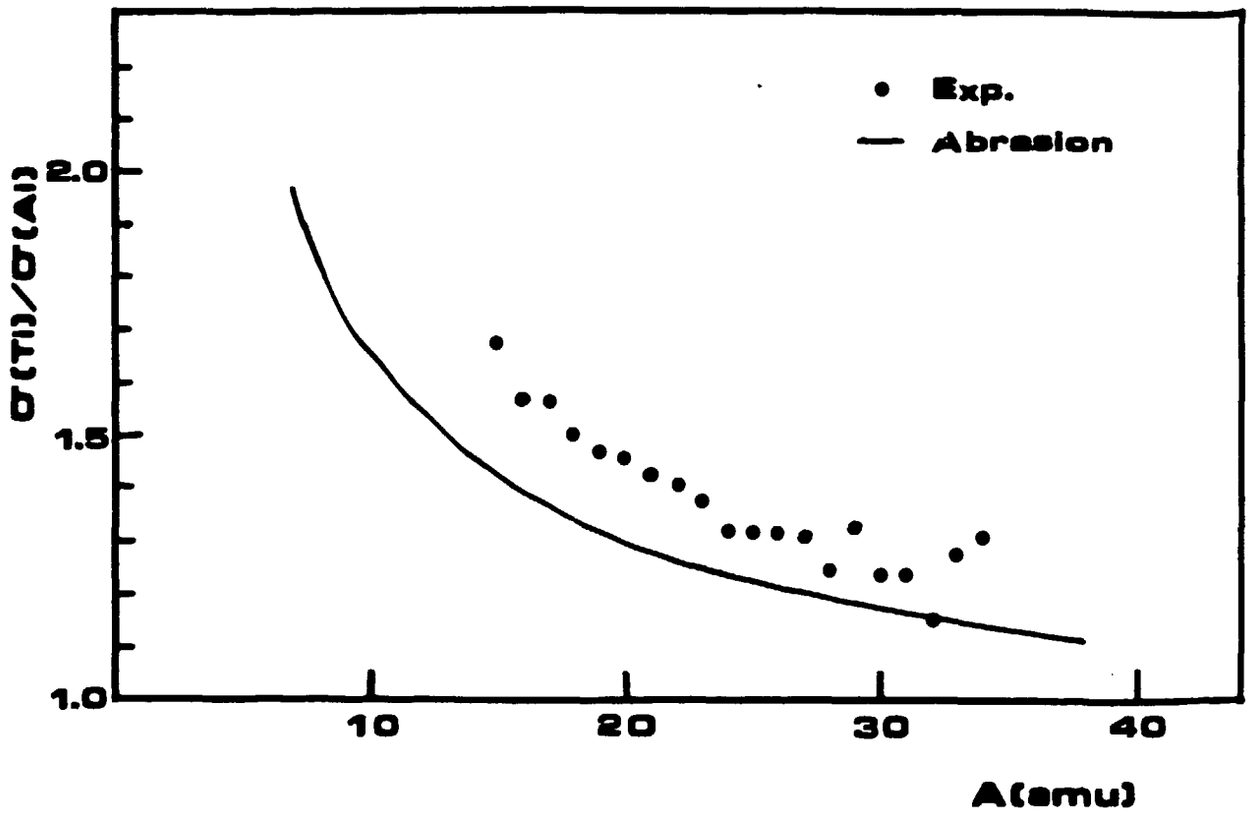

Fig. 7 : Ratios of the mass yields between the $^{40}Ar + ^{nat}Ti$ and $^{40}Ar + ^{27}Al$ reactions. The solid line is the prediction of the clean cut abrasion calculation.

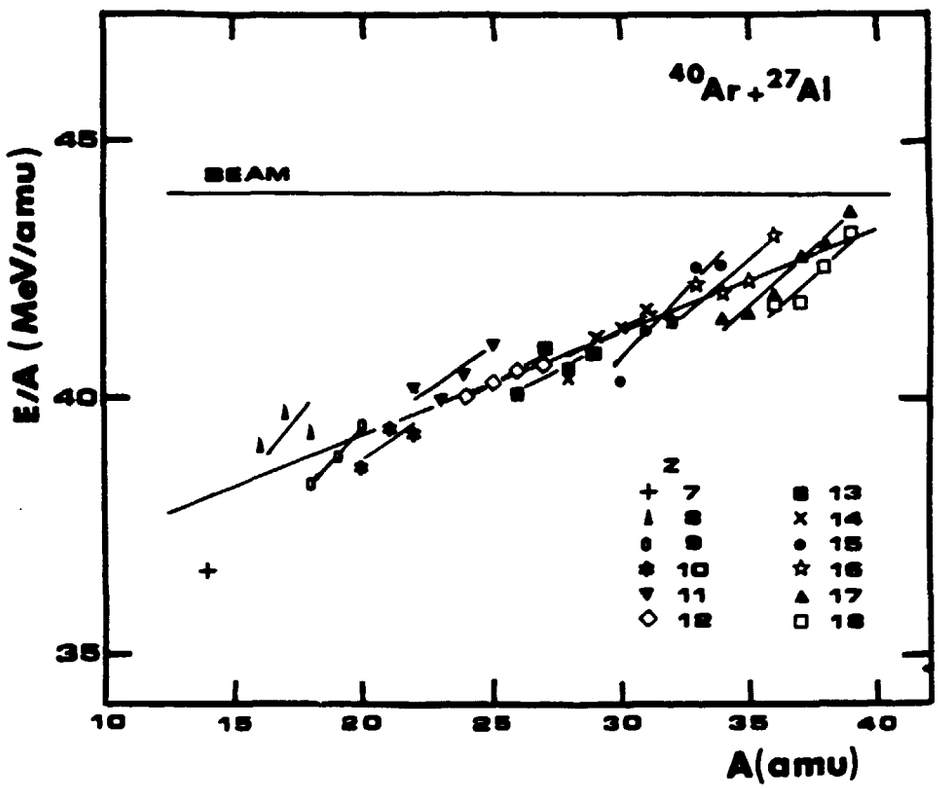

Fig. 8 : Most probable energy of the fragments in MeV/u as a function of their mass.

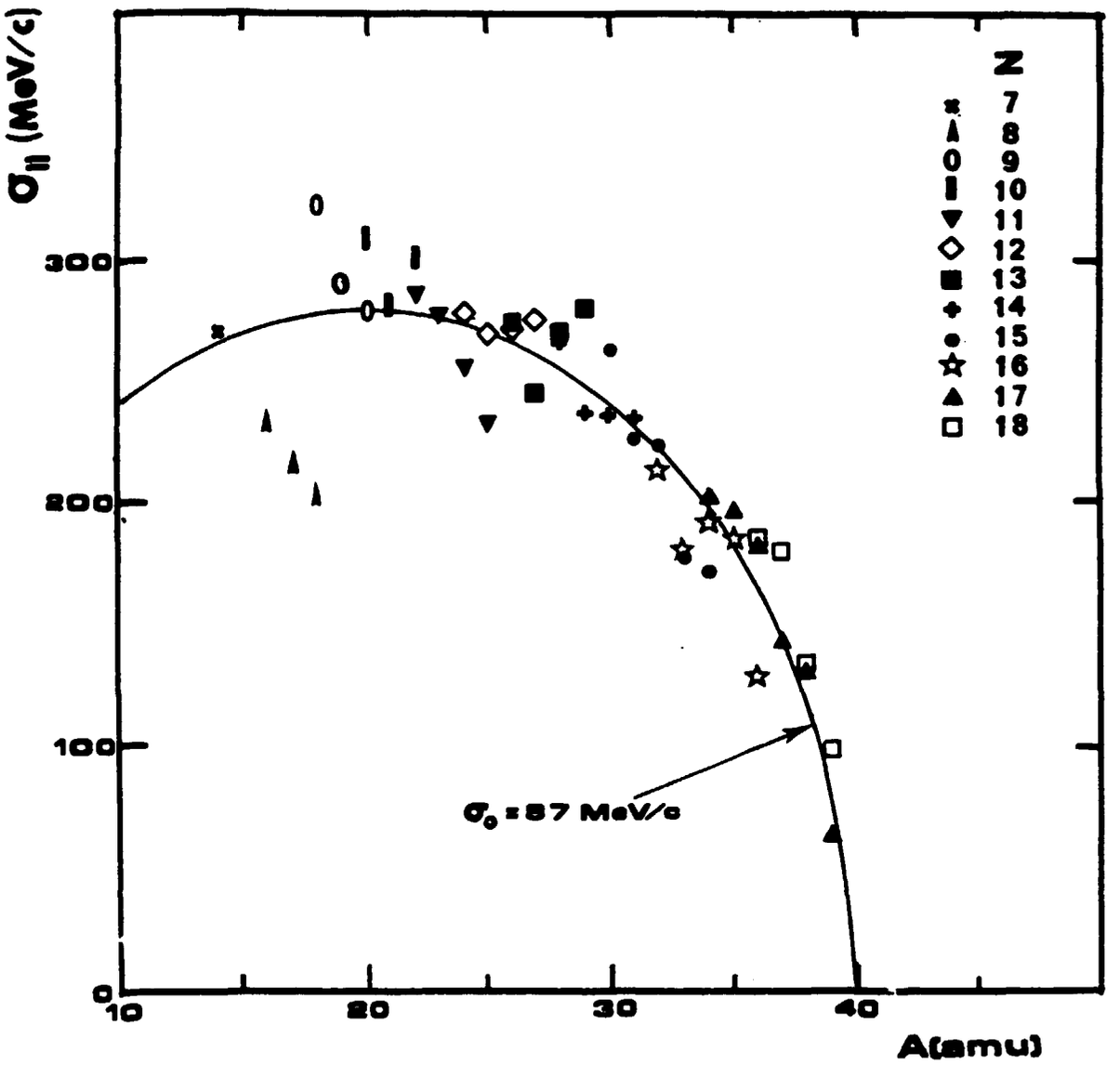

Fig. 9 : Longitudinal momentum variances as a function of the fragment mass for the reaction $^{40}Ar + ^{27}Al$. The general trend of the data is well reproduced by the parabolic law (2) taking σ_0 = 87 MeV/c.

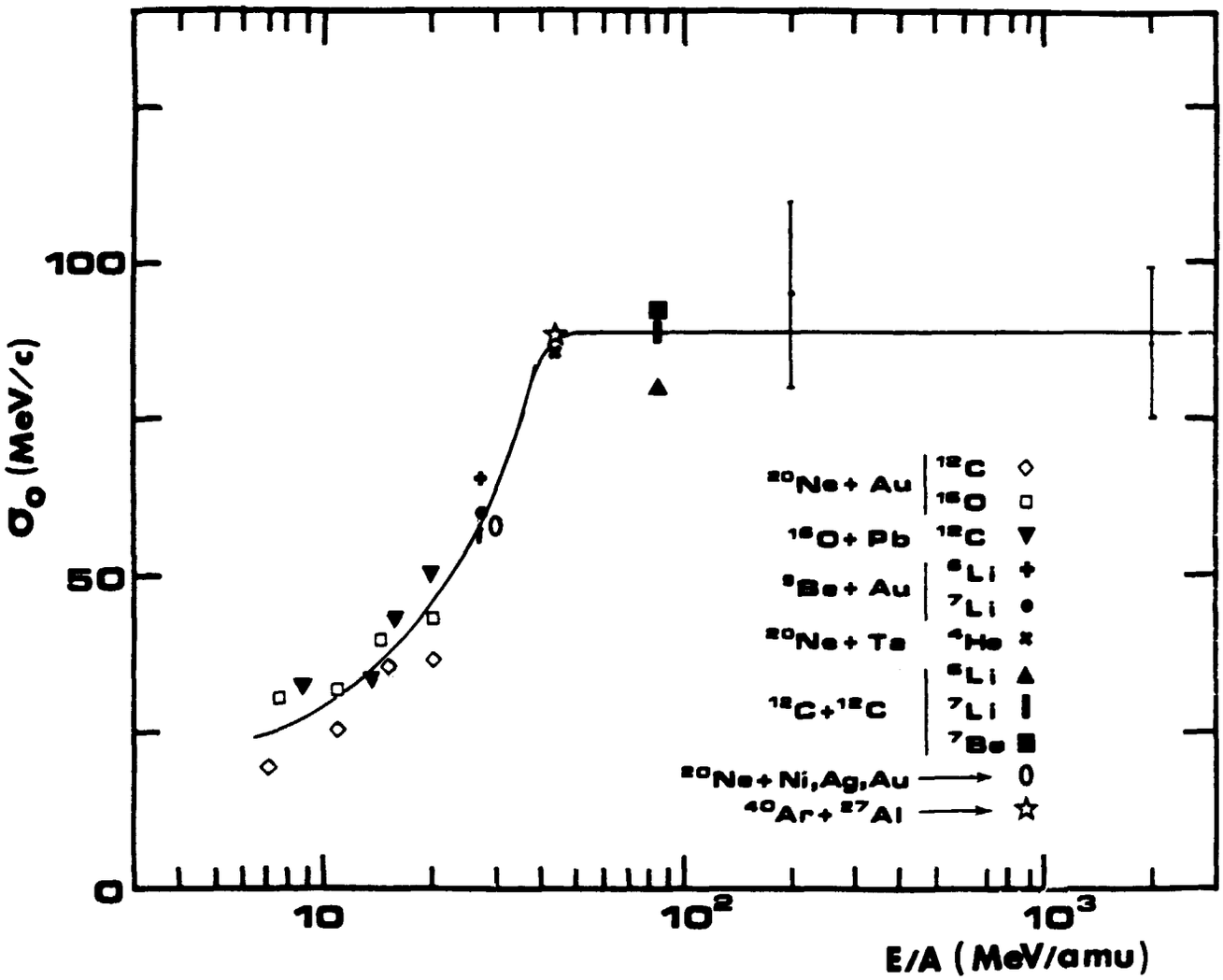

Fig. 10 : Evolution of σ_0 with projectile energy in MeV/u.

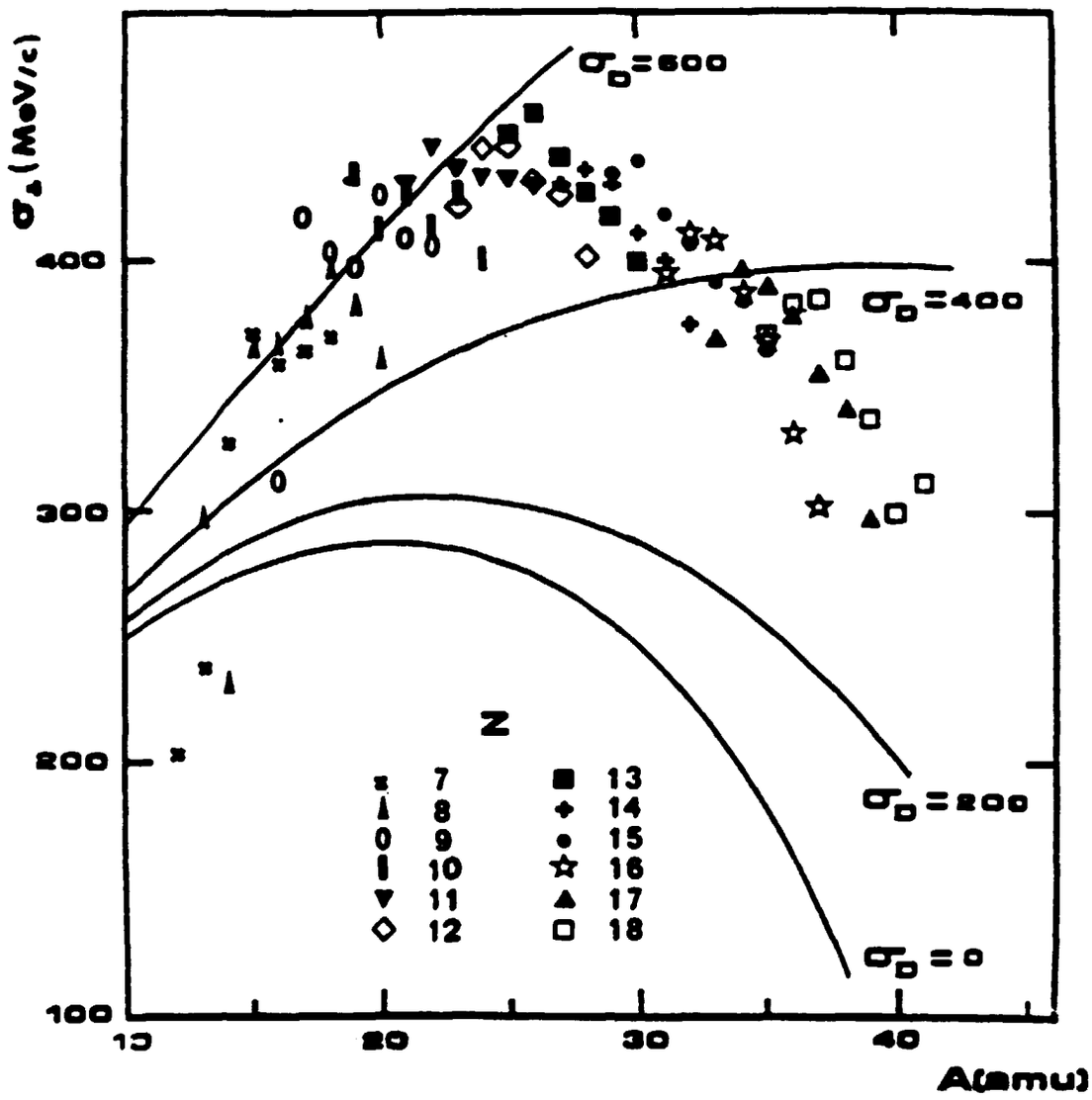

Fig. 11 : Transverse momentum variances as a function of the fragment mass. The curves are the predictions of relation (6) using different values of σ_D

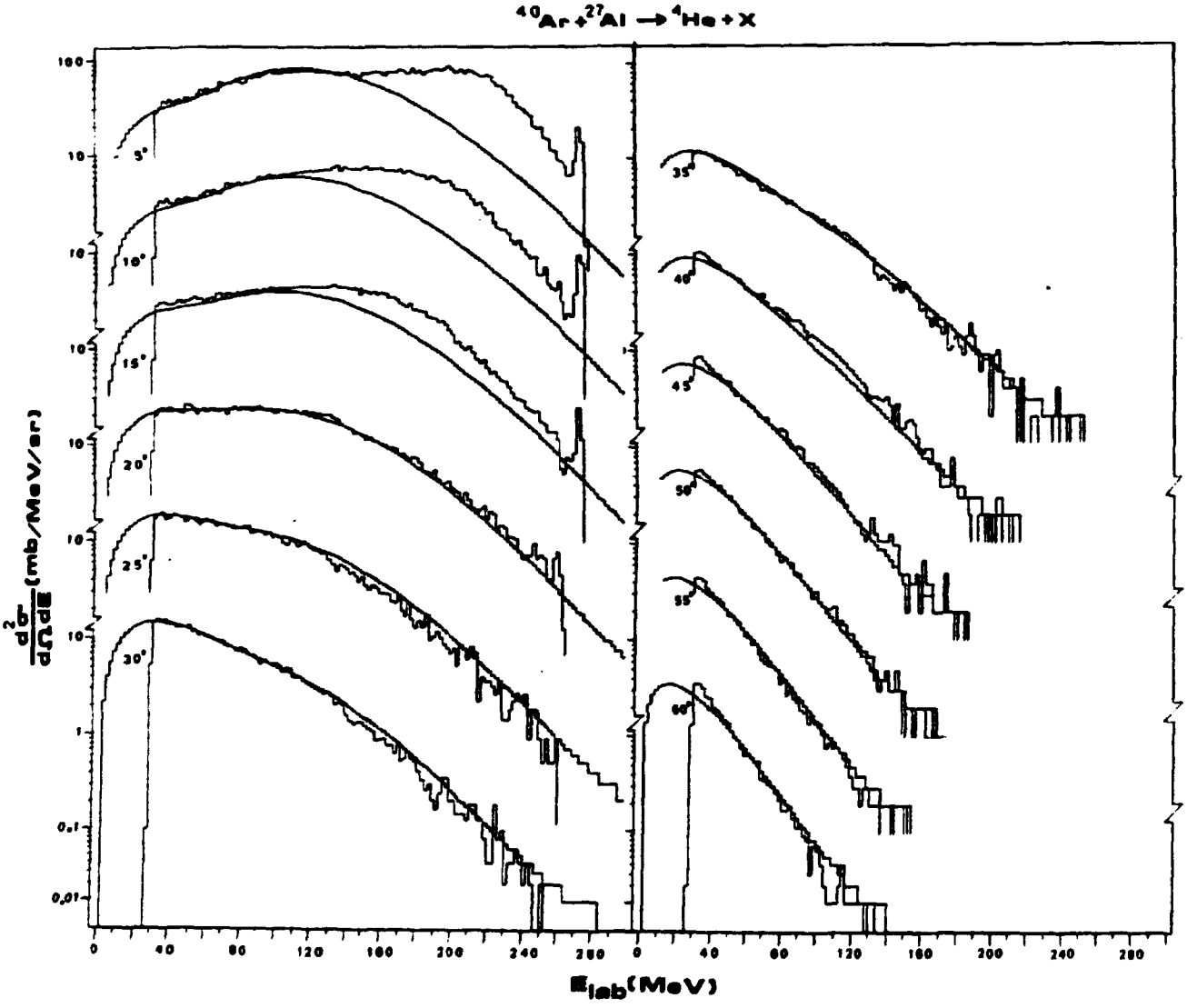

Fig. 12 : Energy spectra of alpha particles from the reaction $^{40}Ar + ^{27}Al$ at E/A = 44 MeV. The solid lines correspond to the two moving source fit described in the text.

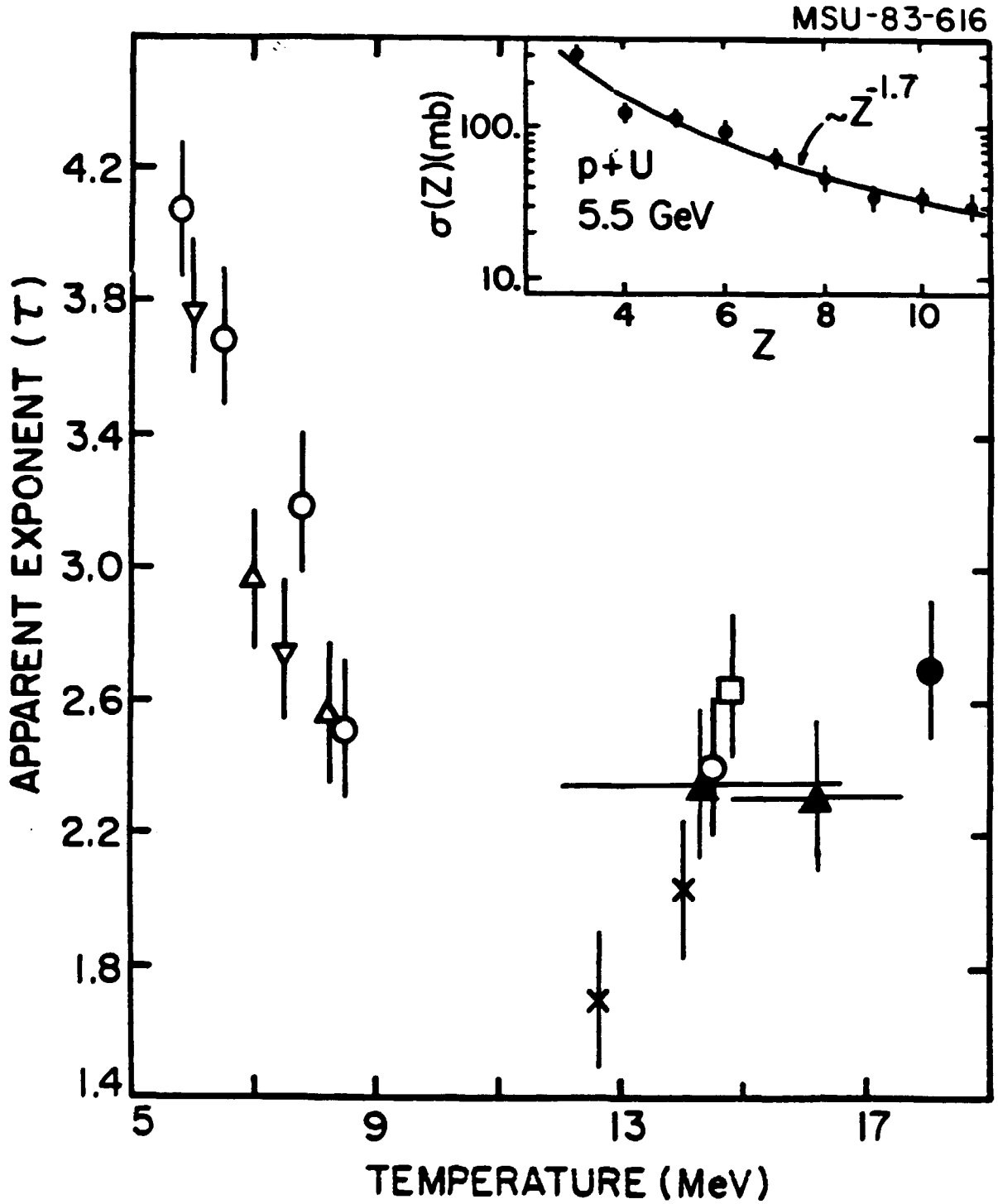

Fig. 13 : The apparent exponent τ of the power law fit to the fragment distributions as a function of the temperature. Our data points (black triangles) have been added to the figure of ref. 50.

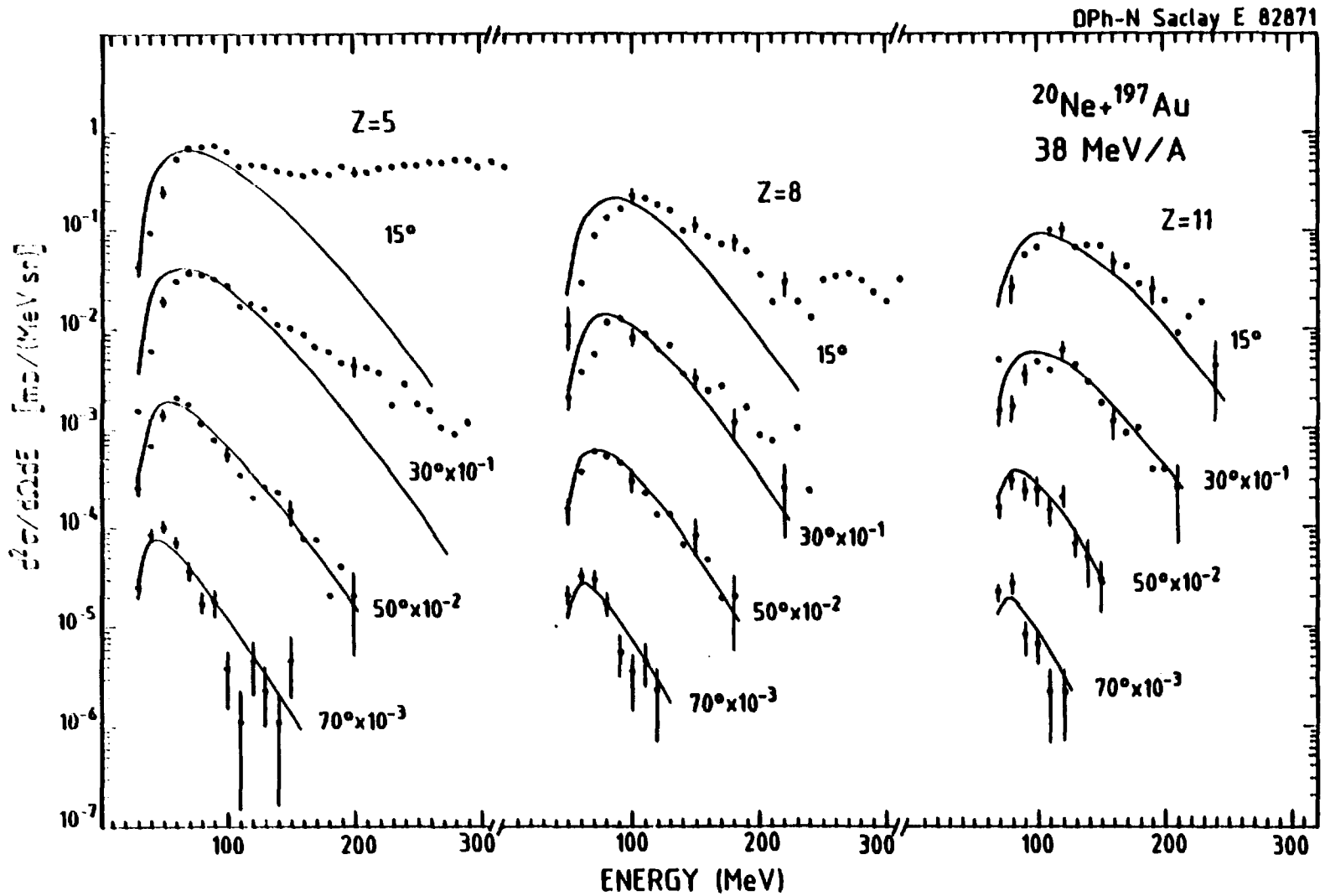

Fig. 14 : Energy spectra of B, O and Na nuclei produced in ^{20}Ne induced reactions on ^{197}Au at E/A = 38 MeV. The solid lines correspond to fits with moving source parametrization of eq. (8).

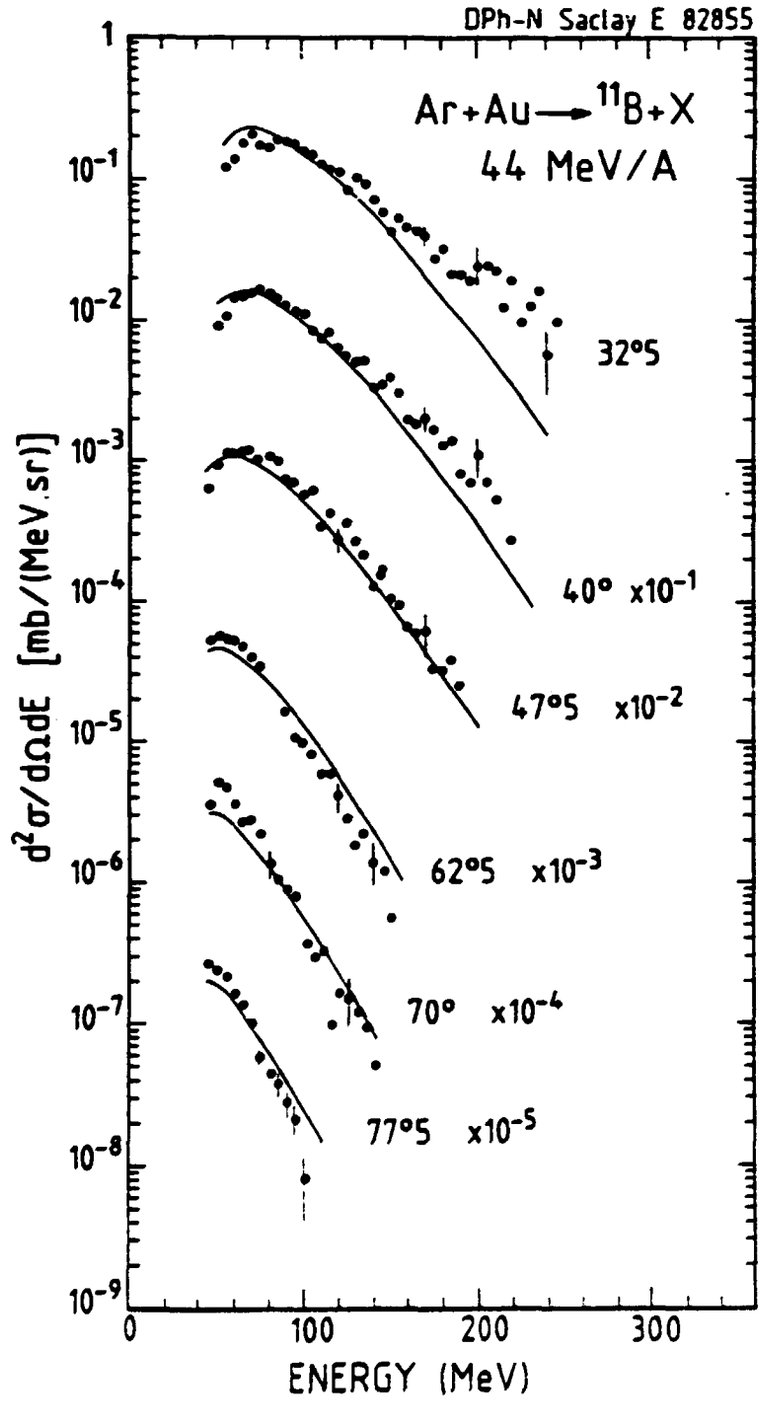

Fig. 15 : Energy spectra of ^{11}B produced in ^{40}Ar induced reactions on ^{197}Au at E/A = 44 MeV. The solid lines correspond to a fit with the moving source parametrization of eq. (8).

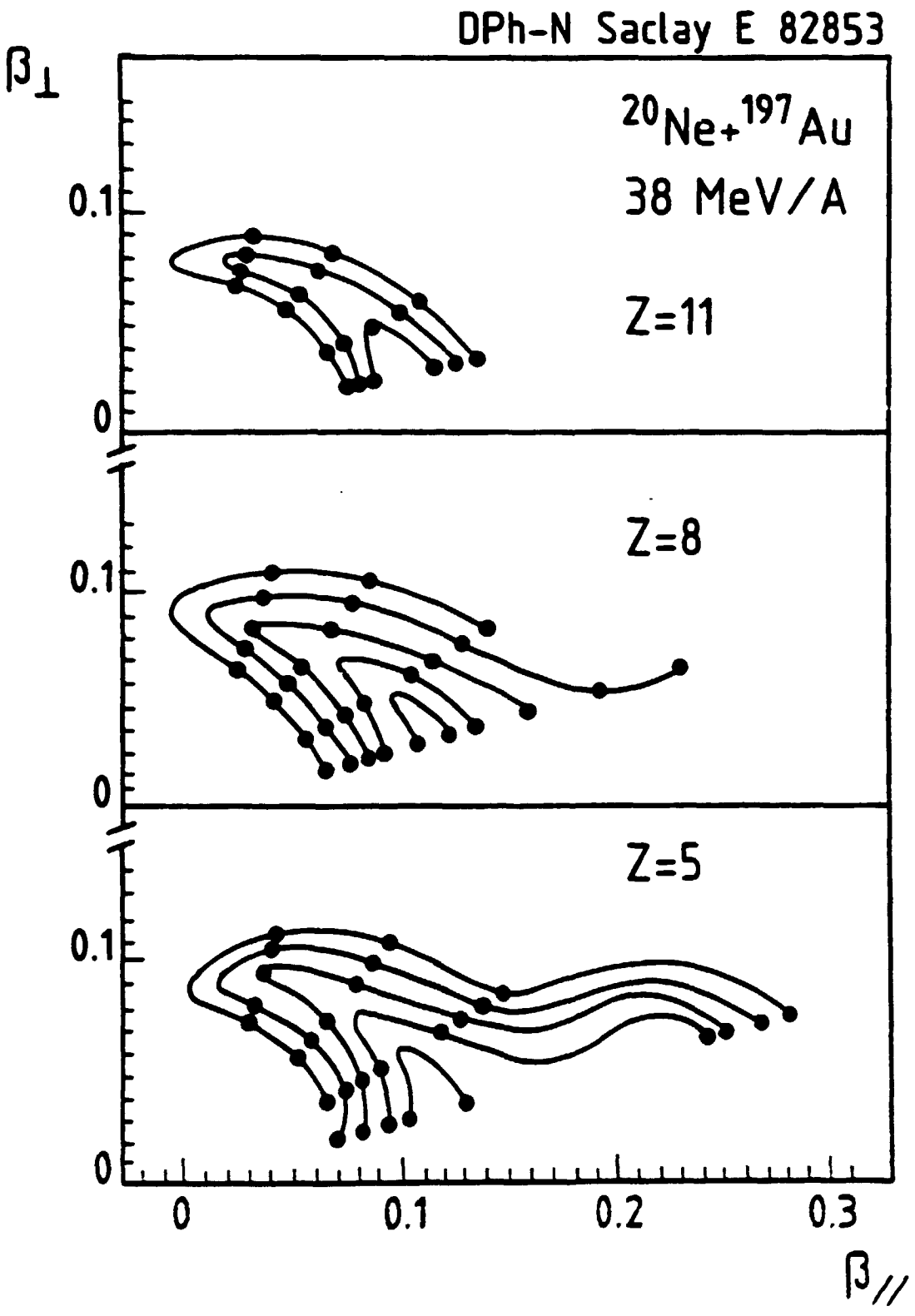

Fig. 16 : Contour plots of invariant cross sections for B,O and Na nuclei produced in ^{20}Ne induced reactions on ^{197}Au at E/A = 38 MeV.

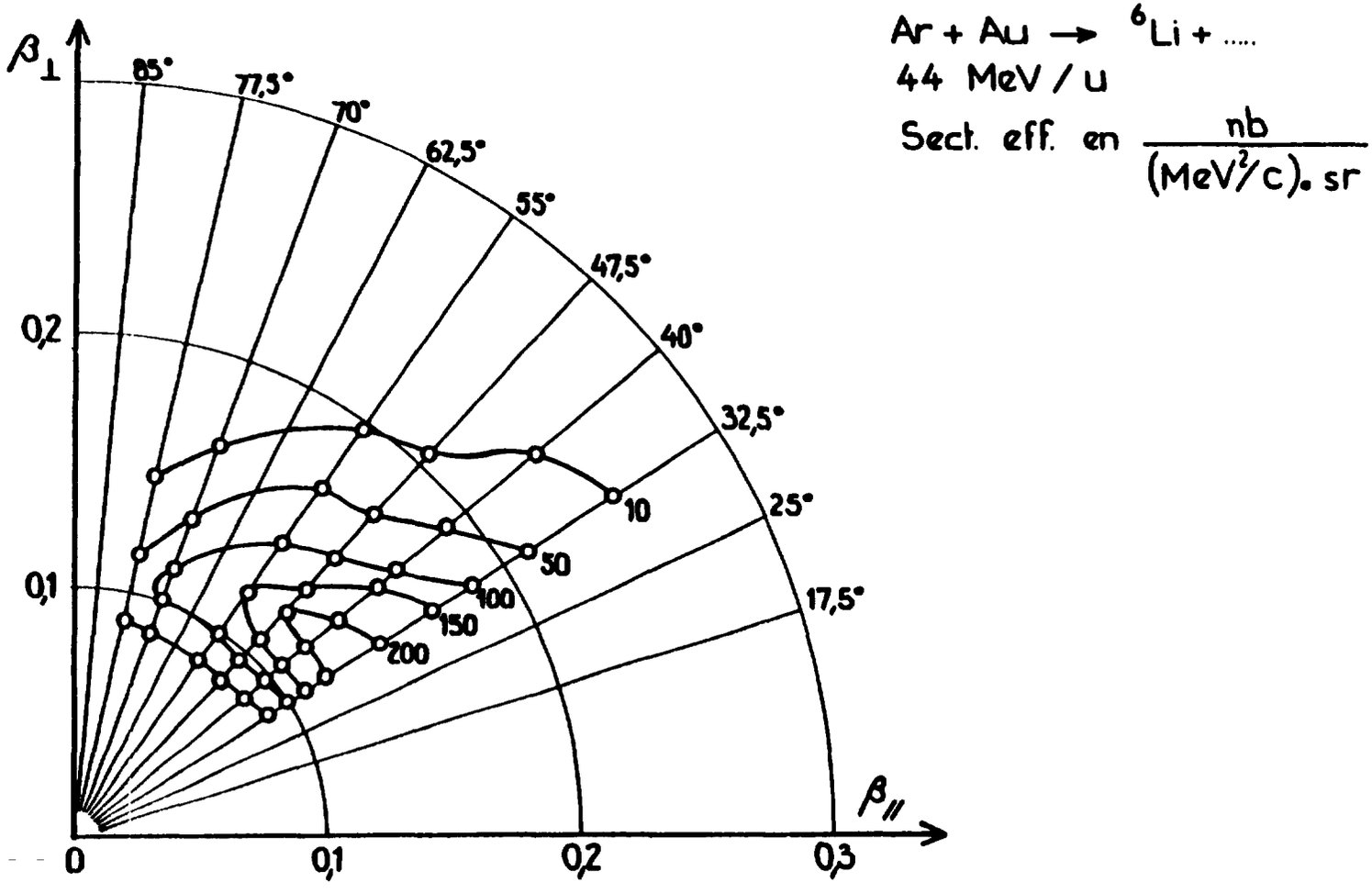

Fig. 17 : Contour plot of invariant cross sections for ^{6}Li fragment produced in ^{40}Ar induced reactions on ^{197}Au at E/A = 44 MeV.

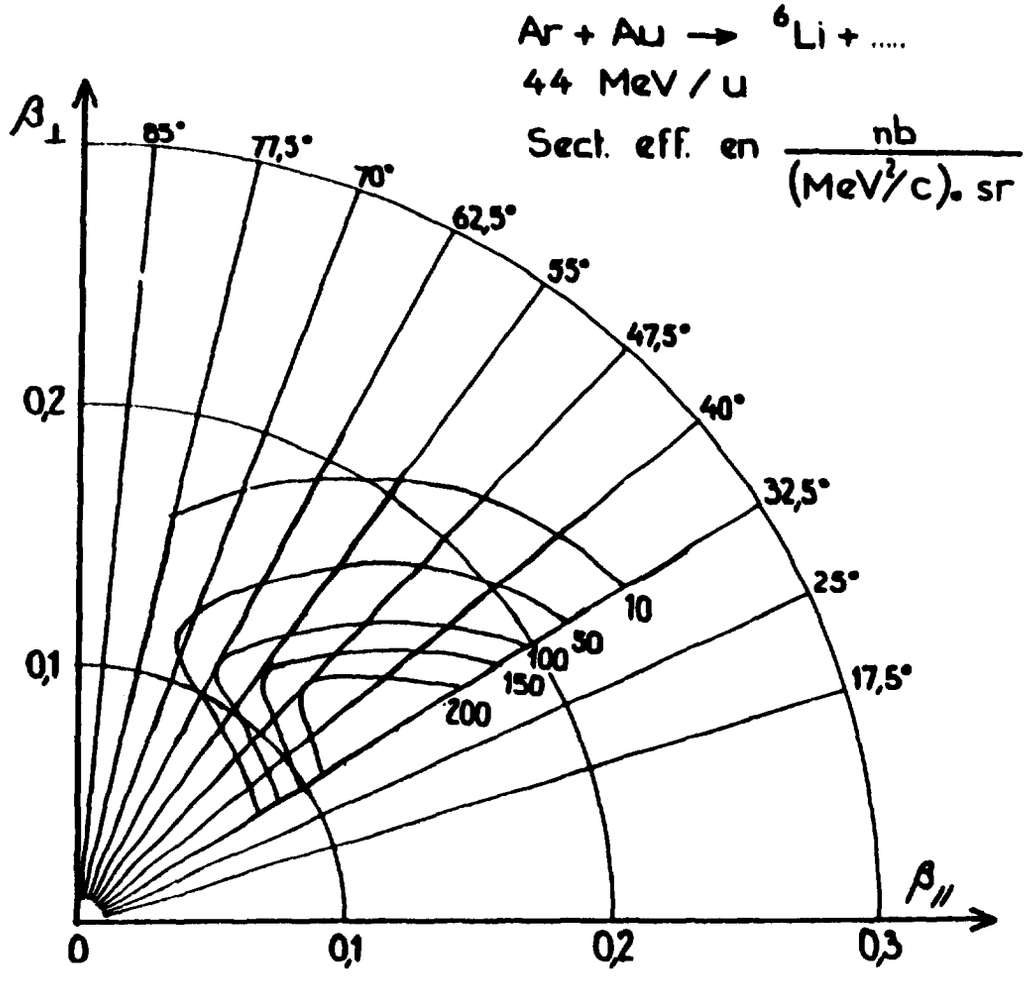

Fig. 18 : Contour plot of invariant cross sections for ^{6}Li resulting from the fit to the data using eq. (8).

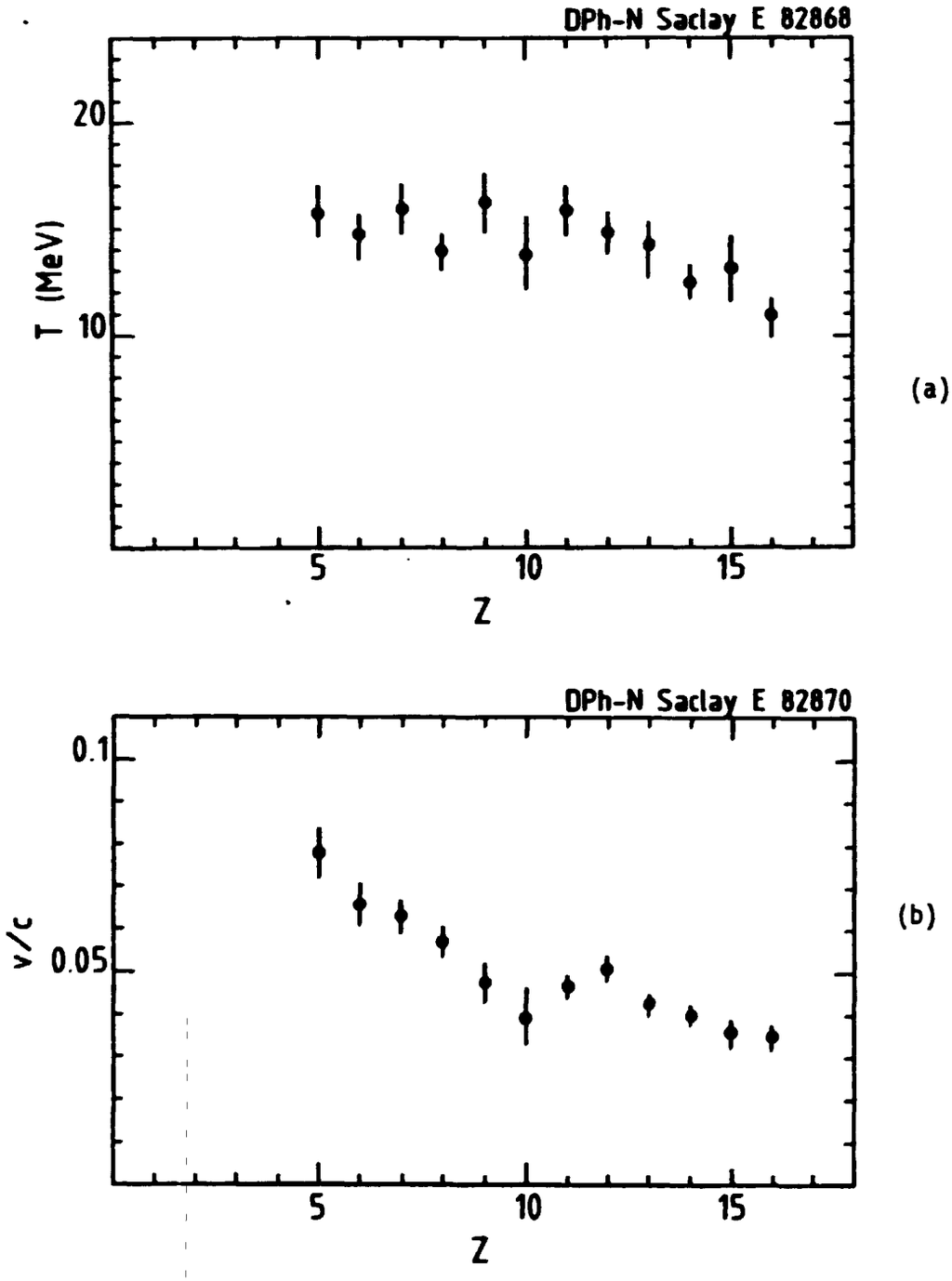

Fig. 19 : Temperatures (a) and source velocities (b) extracted from moving source fits to the energy spectra of fragments produced in ^{20}Ne induced on ^{197}Au at E/A = 38 MeV.

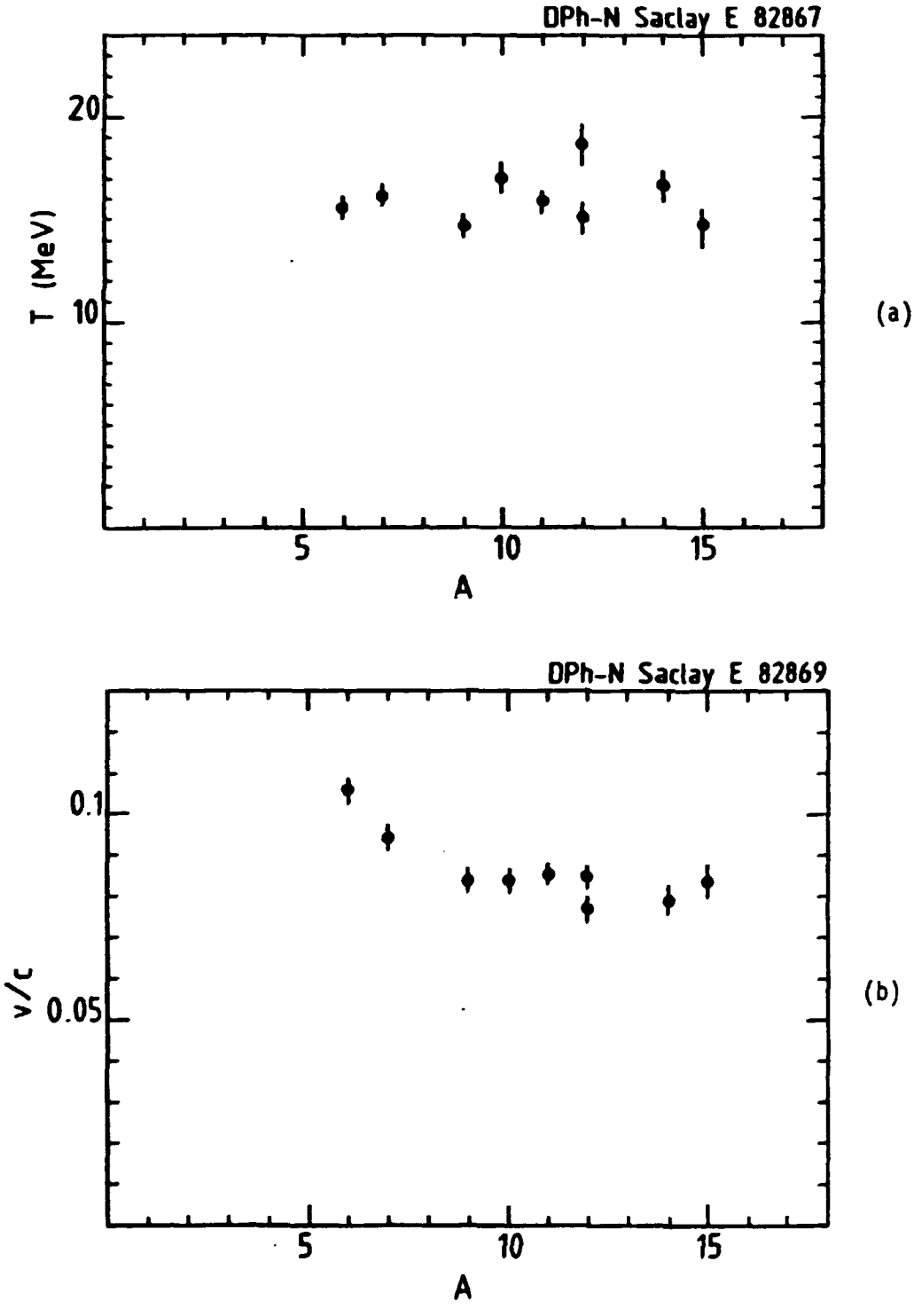

Fig. 20 : Temperature (a) and source velocities (b) extracted from moving source fits to the energy spectra of fragments produced in ^{40}Ar induced reactions on ^{197}Au at E/A = 44 MeV.

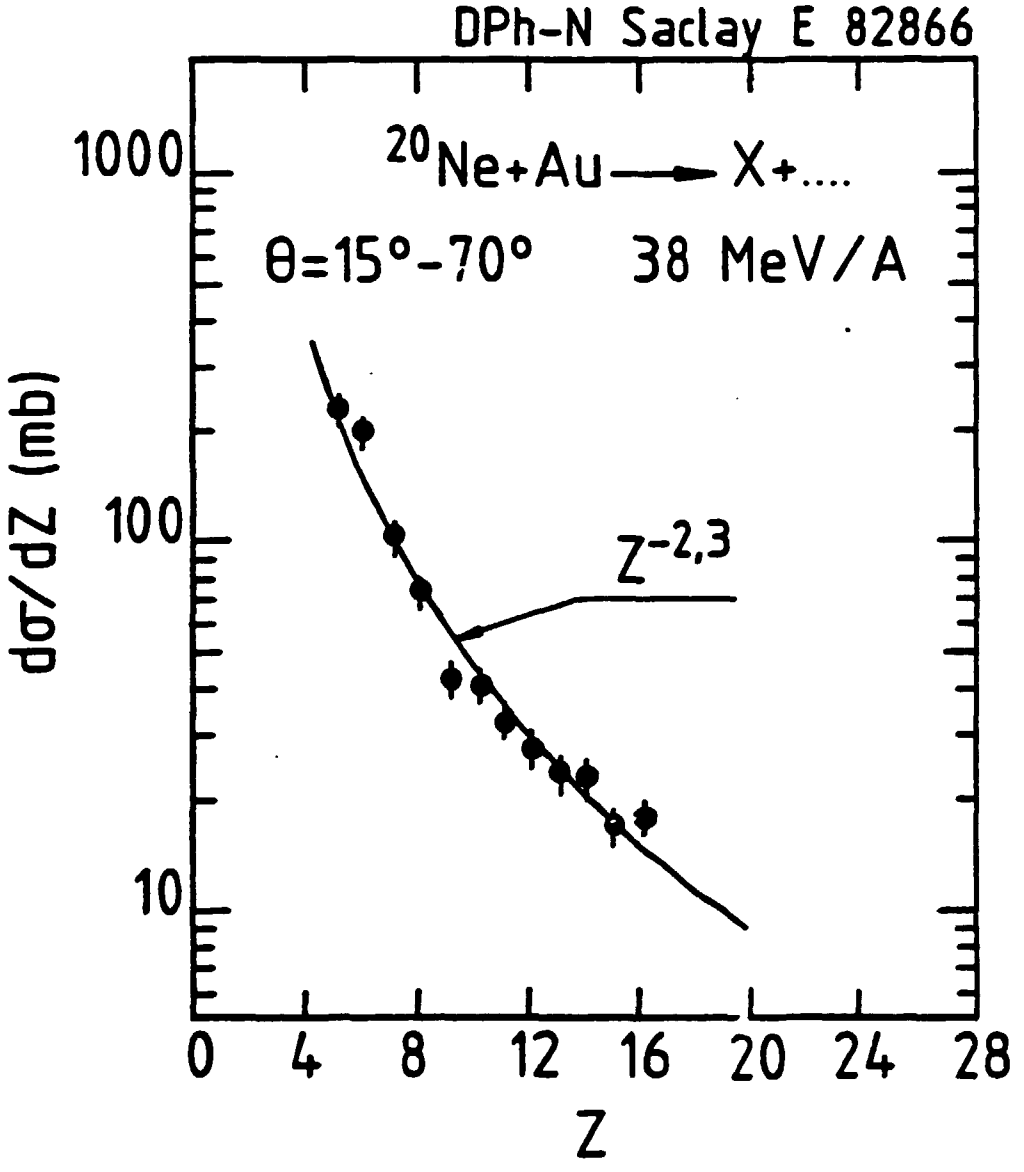

Fig. 21 : Fragment cross sections as a function of fragment charge for the ^{20}Ne + ^{197}Au reaction compared to a power law distribution.

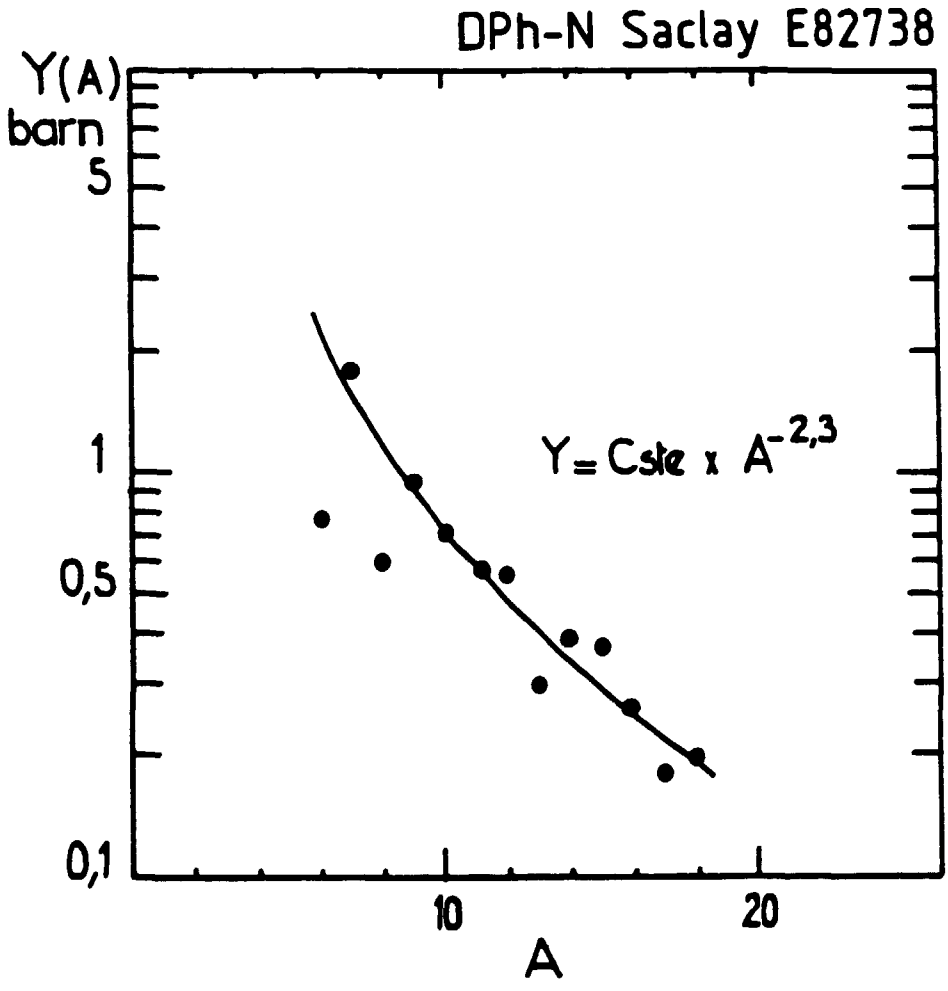

Fig. 22 : Fragment cross sections as a function of fragment mass for the $^{40}Ar + ^{197}Au$ reaction compared to a power law distribution.

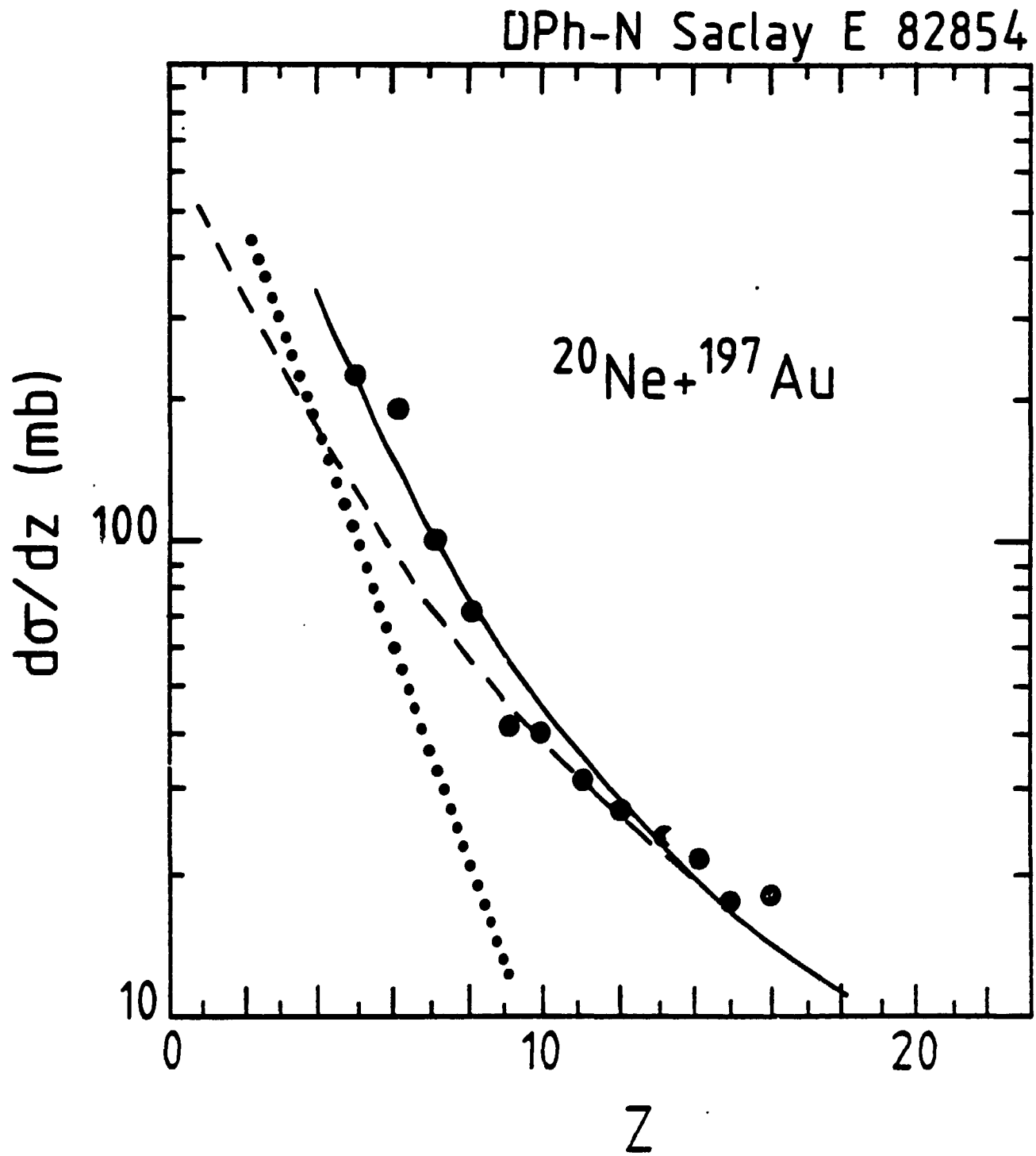

Fig. 23 : Fragment cross sections as a function of fragment charge for the ^{20}Ne + ^{197}Au reaction. The dotted and dashed lines correspond to the evaporation and fragmentation contributions respectively. The solid line is the sum of these two contributions with arbitrary normalization coefficients.

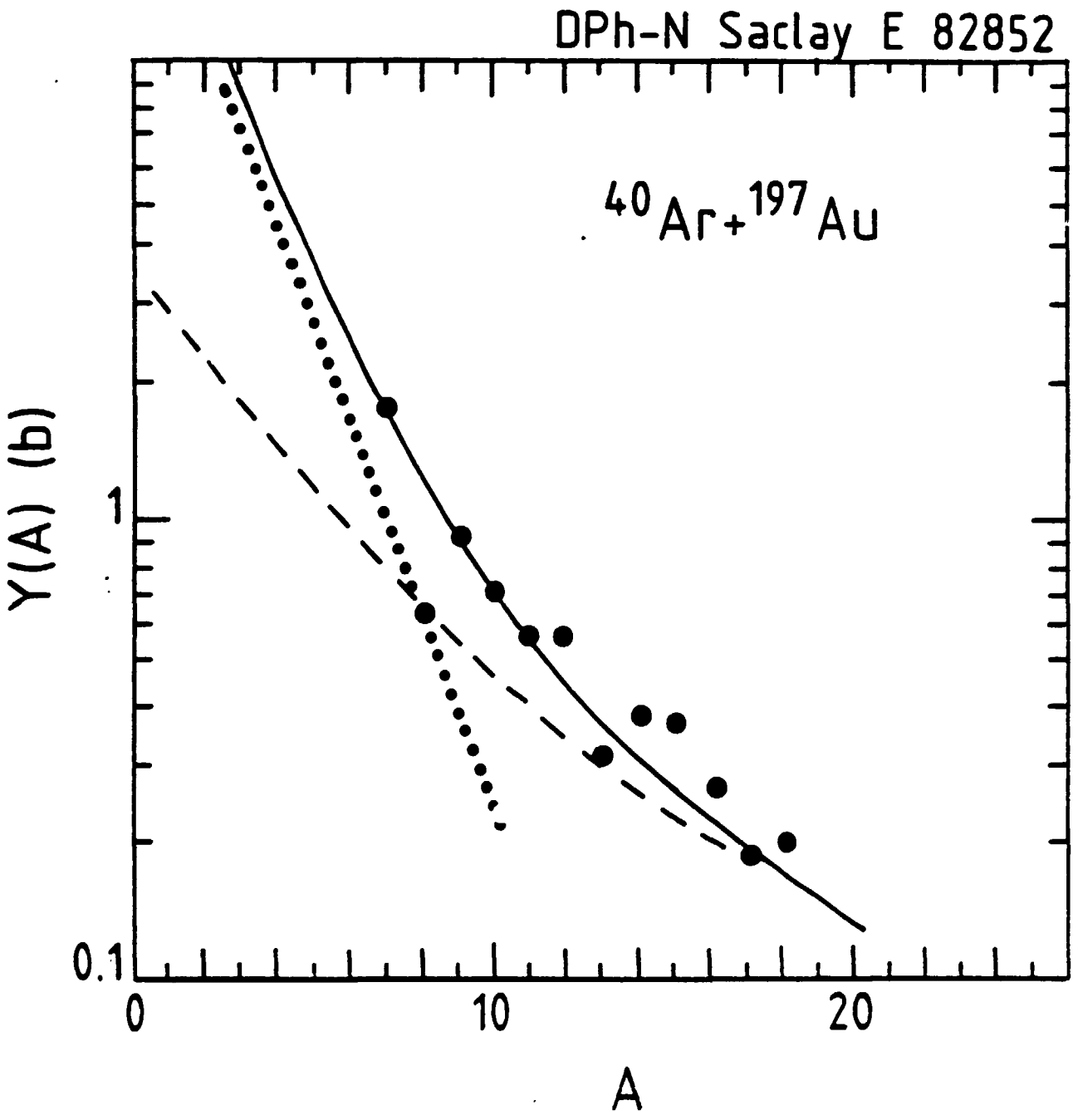

Fig. 24 : Fragment cross section as a function of fragment mass for the $^{40}Ar + ^{197}Au$ reaction. The dotted and dashed lines correspond to the evaporation and fragmentation contributions respectively. The solid line is the sum of these two contributions with arbitrary normalization coefficients.